Consequence Analysis of Residual Water in a Storage Canister – Preliminary Report

Spent Fuel and Waste Disposition

Prepared for
U.S. Department of Energy
Spent Fuel and Waste Science and Technology

Pavan Shukla
Robert Sindelar
Poh-Sang Lam

September 20, 2019

Milestone No. M2SF-19SR010201055
SRNL–STI–2019–00495

Prepared by
Savannah River National Laboratory
Savannah River Nuclear Solutions
Aiken, South Carolina 29808

Savannah River National Laboratory is a multiprogram laboratory managed and operated by Savannah River Nuclear Solutions, LLC, for the U.S. Department of Energy under contract DE-AC09-09SR22505.

EXECUTIVE SUMMARY

This report describes an investigation of materials' interactions due to residual water remaining inside a dry storage canister, and the impacts on the spent nuclear fuel and canister internals.

Recent findings from the High Burnup Demonstration project, and an Integrated Research Project, sponsored under the DOE-Nuclear Energy, Spent Fuel and Waste Disposition campaign, show that residual free water, well above the amount of approximately 0.4 gm-moles that had been assumed for a 3 torr rebound pressure, may remain within an SNF canister following prototypic drying.

The impacts on the fuel and canister internals, with a focus on the oxidation of the cladding and of postulated exposed fuel, were evaluated using an integrated set of time-dependent environmental conditions with semi-empirical materials oxidation kinetics models. This "integration model," previously developed and used by the Center for Nuclear Waste Regulatory Analysis for the U.S. Nuclear Regulatory Commission, was applied and expanded with improved sub-models for water radiolysis, and for cladding and fuel oxidations.

The materials and conditions considered in the analyses in this report:

- Free water content: 5.5 and 10 moles (present as pooled water and/or water vapor)
- Bound water content: potential presence on CRUD acknowledged, but bound water thermal decomposition release, and/or radiolytic gas yield were not considered
- Cladding alloys: Zircaloy-4, ZIRLO, M5
- Fuel pellet: UO_2
- Breached fuel assumptions: Up to 4 failed rods per canister based on 0.1% cladding failure rate
- Temperature: Canister zone-dependent, time-dependent temperatures with 400°C peak temperature condition
- Radiation: 2.0×10^{14} (low dose rate) and 3×10^{15} (high dose rate) eV/g/s

Phenomena evaluated include:

- Water radiolysis creating H_2 and O_2
- Cladding oxidation – additional oxidation (post-discharge) with alloy-dependent models
- Fuel pellet oxidation – additional oxidation (post-discharge) from UO_2 to U_4O_9 to U_3O_8 with fuel burnup-dependent oxidation model
- Cladding rupture due to fuel oxidation, with a critical strain criterion for cladding
- Flawed cladding crack extension under fracture condition, with a K_{IC} criterion for cladding

The primary observations, results and conclusions:

- Radiolysis of water will cause time-dependent production of H_2 and O_2
- Hydrogen build-in will occur; however, oxygen will be limited due to consumption in oxidation reactions, and would not be expected to reach above the limit of 5 volume % for oxygen control to avoid reaching flammable gas compositions
- Oxygen will be consumed by zircaloy and fuel pellet oxidation. The partitioning of oxygen to fuel cladding vis-à-vis fuel pellets is dependent on cladding alloy and number of fuel breaches
- Increase in breached cladding opening area and crack mouth displacement can occur due to fuel pellet oxidation and swelling at conditions dependent on cladding alloy, temperature, and initial water content

Two cladding failure evaluation methodologies were applied. The first methodology assumed a critical (failure) strain criterion (~6.5%) for all the cases of cladding alloys. The second evaluation methodology involved considering crack extension using linear elastic fracture mechanics. Two K_{IC} fracture toughness

levels of 25 and 90 MPa√m were applied. This second methodology is more limiting, i.e., less strain than the 6.5% failure strain is needed to cause cladding failure; this also should be more accurate in predicting the cladding response under fuel pellet oxidation and mechanical loading of the cladding at a breach location. The second approach can also be used to estimate crack opening width to allow an estimate of potential release of fuel pellet fines and gaseous/volatile fission products to the canister cavity.

The primary conclusion from this investigation is that no major degradation of fuel and canister internals will occur within the canister for the bounding conditions of inadvertent residual water assumed for this report. Specifically, no fuel reconfiguration significant to criticality control, and no major loss of fuel assembly/canister internals significant to fuel retrievability are expected. Fuel cladding breach area increase and the loss of fuel particles from the rod to canister internals may be anticipated for the cases of initially failed (breached) rods at both water levels, but not for rods with no initial breaches. The extent of fuel particle loss from the breached fuel rod, and increase in the canister radiological source term were not evaluated in this present work.

The term “failure risk” is used throughout this report in comparing cases (set of thermal, radiation, cladding type, etc conditions) aggressive to cause fuel pellet oxidation leading to predicted extension of an initial breach area opening. That is, a case that would cause more fuel oxidation than another case would be deemed to have a higher failure risk. This is not the classic definition of risk, i.e., Risk = Consequence x Probability.

Due to limitations in available data, the inputs to the integration model relied on best available data and assumptions. Additional activities are recommended to refine this preliminary work to enable determination of radiological source term increase from fuel release into the canister due to increased cladding breach opening due to inadvertent residual water in a canister loaded with breached rods.

This report fulfills the M2 milestone M2SF-19SR010201055, “Consequence Analysis of Water in Cask” under Work Package Number SF-19SR01020105.

CONTENTS

LIST OF FIGURES

LIST OF TABLES

ACRONYMS

BWR	Boiling Water Reactor
CNWRA	Center for Nuclear Waste Regulatory Analysis
CANDU	Canada Deuterium Uranium
DOE	US Department of Energy
HBU	High Burn-Up
IRP	Integrated Research Project (type of NEUP)
LWR	Light Water Reactor
NE	Nuclear Energy
NEUP	Nuclear Energy University Program
NRC	Nuclear Regulatory Commission
PWR	Pressurized Water Reactor
PNNL	Pacific Northwest National Laboratory
RH	Relative Humidity
SFWD	Spent Fuel and Waste Disposition
SNF	Spent Nuclear Fuel
SNL	Sandia National Laboratories
SRNL	Savannah River National Laboratory

ACKNOWLEDGMENTS

The authors acknowledge U.S. Nuclear Regulatory Commission staff member Drs. Tae Ahn and Ricardo Torres for their direct contributions to, and insightful discussions during the preparation of this report. The authors also acknowledge various current and previous staff members of Center of Nuclear Waste Regulatory Analyses (CNWRA) including Drs. Hundal Jung, Lynn Tipton, Kaushik Das, Xihua He and Debashis Basu. Dr. Pavan Shukla, the lead author of this report, was a previous staff member of CNWRA, and along with the acknowledged personnel, worked on the previous work entitled "Extended Storage and Transportation: Evaluation of Drying Adequacy" that evaluated impact of residual water on a Spent Nuclear Fuel dry storage canister internals. Several ideas and concepts in this work are borrowed from the previous work.

Special acknowledgments to Drs. Tae Ahn and Hundal Jung for the fuel oxidation model and cladding rupture (strain) criterion and for their contributions in developing the integration model in the previous work. In addition, special acknowledgements to Drs. Kaushik Das and Debashis Basu for the zone approach to track fuel and cladding temperatures and their evolution in the storage canister in the previous work. Also, special acknowledgments to Dr. Lynn Tipton for his contributions in developing radiolysis model in the previous work. The fuel oxidation model and cladding rupture criterion were augmented in the present work, and the zone approach and radiolysis model were used with additional bases. The authors acknowledge Dr. Ricardo Torres for discussions on the commercial fuel drying process, and fuel and cladding temperatures during storage. The authors also acknowledge Ron Kesterson for technical review of this report and Dr. Charles Bryan for his contributions for the estimation of residual water and for his numerous improvements to literary quality.

This page intentionally left blank.

1. INTRODUCTION

Dryness of spent nuclear fuel (SNF) and the surrounding environment in a canister is an essential aspect in evaluation of materials aging during extended dry storage. Recent work (Bryan et al., 2019) suggests that inadvertent free water may remain following drying even with a dryness criterion of 3 torr pressure limit following a 30-minute hold after active drying is completed. Regulations in 10 CFR Part 72 require that for a period of at least 20 years the dry storage casks function to ensure (i) fuel assemblies can be retrieved if necessary,[1] (ii) subcritical conditions can be maintained under credible scenarios, (iii) radioactive releases do not exceed specified limits, and (iv) there is sufficient shielding to keep direct radiation dose rates below specified limits. To this end, an evaluation of the drying adequacy {impact of selected inventories of free water on loaded SNF in a multi-purpose canister} was prepared by the Center for Nuclear Waste Regulatory Analyses (CNWRA) in 2013. The CNWRA work was conducted with assumption that free water could range between 5 to 55 moles and included estimating extent of fuel and cladding oxidation due to radiolytic decomposition of the free water. Although, the work also included bound water estimates, no effort was made to account for bound water's radiolytic decomposition and subsequent impact on fuel and cladding oxidation.

The present work under the DOE NE Spent Fuel and Waste Disposition, Storage and Transportation campaign was conducted to update and broaden the CNWRA work to provide a comprehensive topical investigation on the impacts of residual water in an SNF canister, especially with the aim of refining the estimation of the likely amounts of inadvertent residual water, and the extent of oxidation of fuel, including HBU fuel, and cladding oxidation.

The overall goal of the investigation is to evaluate the (potential adverse) impact of residual water on the fuel and canister internals. The work to date shows that the only potentially significant impact is an increase of the canister radiological source term due to fuel (fines) that may be released at a breached location that extends from a fiducial size of a 1 mm hole to a greater size as fuel oxidation would occur. Thus, the focused objective of this present work is to develop a methodology for the estimation of a potential radiological source term increase due to the increase in the oxidized SNF matrix, i.e., formation of U_3O_8 and release of fines through the cladding with an extended breach.

The previous CNWRA work estimated that 55 moles of free water could form 270 g of U_3O_8, which can cause gross rupture of cladding and release of high-level radioactive elements and their oxides in the canister cavity. Thus, residual water has potential to change the fuel's condition which in turn complicates fuel retrievability and recertification of the storage canister after the initial 20-year license. In addition, although the CNWRA work accounted for fuel oxidation, no discrimination was made between fuel burnup levels and their effects on extent of fuel oxidation. This present work differs with the CNWRA work in following respects:

- Cladding oxidation models were developed using the rate constants reported in the literature for various cladding alloys in air and in the dry storage temperature range. The cladding oxidation rates used in the present work are lower than the rates used in the CNWRA work.

[1] NRC ISG-2, Rev. 2 stipulates the following for fuel retrievability: "ISG-2, Rev. 2 defines ready retrieval as 'the ability to safely remove the spent fuel from storage for further processing or disposal.' In order to demonstrate the ability for ready retrieval, a licensee should demonstrate it has the ability to perform any of the three options below. These options may be utilized individually or in any combination or sequence, as appropriate.
A. remove individual or canned spent fuel assemblies from wet or dry storage,
B. remove a canister loaded with spent fuel assemblies from a storage cask/overpack,
C. remove a cask loaded with spent fuel assemblies from the storage location"

- A burnup-dependent fuel oxidation model was developed. The model accounted for inhibition effect of fission products on fuel oxidation rates.

- A strain-based criterion was used to determine the cladding failure condition. A failure condition would exist when a sufficient amount of fuel oxidation (at a postulated breached clad location) causing fuel pellet swelling to load the cladding had occurred.

- An alternative criterion, a fracture mechanics-based criterion, was developed to determine the threshold strain for cladding failure. Formulation of the fracture mechanics-based criterion also yielded crack size parameters such as opening area which is needed to estimate fines' release in a canister cavity.

An estimation of the amount of release of fuel fines from cladding that has had its cladding breach extended due to fuel pellet oxidation has not been attempted in this present work. An estimation of fines release is expected to be tractable through an opening size that can be estimated through the fracture mechanics formalism. Additional refinements to this work culminating in the estimation of increase of the radiological source term in the canister cavity are suggested.

2. OBJECTIVE AND SCOPE

The objective of this work is to examine the consequences of a residual water on change in condition of cladding and SNF during dry storage. Small amounts of residual water may remain in SNF dry storage canisters after the fuel assemblies are transferred to the canister in the spent fuel pool (SFP), the canister is removed from the SFP and drained or pumped, vacuum dried in several pressure reducing steps, and backfilled with helium. This residual water from incomplete drying could degrade fuel rod cladding, oxidize exposed fuel pellets, and cause cladding failure resulting in SNF fines' release in canister cavity. If residual water content is high enough, it could corrode internal components inside the canister, e.g., fuel basket, and neutron absorber plates, but CNWRA work indicated that corrosion of the internal component is expected to be negligible even with 55 moles of residual water. Considering this, focus of this work to determine partitioning of residual water towards fuel and cladding oxidation. Residual water will decompose by radiolysis and create reactive oxygen species, which, at sufficient high temperatures will oxidize cladding, and UO_2 exposed by clad breaches. If a significant fraction of UO_2 in a fuel rod is oxidized to U_3O_8, swelling of the fuel pellets will rupture the cladding and release fuel particles, contaminating the inside of the canister and complicating retrieval of fuel assemblies, transport and ultimate disposal.

The report describes an evaluation of the potential cladding and exposed SNF pellets due to residual water. An integrated quantitative approach was used to estimate the effects. The approach consisted of (i) the evolution of environmental conditions, i.e., temperature and radiation field, in the cask, (ii) the physicochemical processes that affect degradation of the materials within the cask, and (iii) the potential damage states that may result from these conditions and processes. The assessment considers the following set of cask environmental conditions: (i) the quantity of residual water after drying, (ii) internal temperature fields and their intensity decrease over time, and (iii) the strength of the internal radiation field. The quantity of residual water will affect the mass of cladding, SNF, and other components that are degraded by oxidation. Temperature controls the rate of the oxidation reactions, the phase composition of water, and, to a lesser extent, the rate at which water vapor is radiolyzed. The strength of the radiation field controls the radiolysis rate of residual water. These processes, i.e., time evolution of temperature fields and their effects on radiolysis of residual water, fuel and cladding oxidations, were modeled using the integrated approach.

Generation of oxygen from radiolysis of residual water is modeled considering first order kinetics for depletion of residual water and uncertainties such as radiolytic decomposition of the products of the residual water. The cladding and SNF oxidation mass action equations are modeled in five time-dependent distinct temperature zones inside the cask's internal volume. At each time step in the integrated assessment, the total amounts of hydrogen and oxygen produced by radiolysis are calculated. A CASTOR V/21 cask was selected for defining five temperature zones to track thermal evolution in a storage canister. For each zone, the oxidized surface area of cladding and the exposed fuel are tracked. Available oxygen is reacted with the cladding and exposed fuel at the temperature for that zone. Oxygen not consumed in a colder zone is transferred to the adjacent warmer zone. This sequence of calculations continues until the oxidation reactions are complete for that time step. Detailed descriptions of the physicochemical process models that control extent and rate of degradation are provided in Section 3, followed by simulation data and results of the integrated analysis in Section 4. Summary, conclusions, and future refinements are discussed in Chapter 5, and references cited in this work are listed in Chapter 6.

3. TECHNICAL APPROACH

3.1 Residual Water Inventory

A drying process is implemented when fuel assemblies are loaded in a dry storage canister. Loading of commercial spent nuclear fuel in a storage canister involves lowering the canister system in a pool, wet transferring of the spent nuclear fuel assemblies in the fuel basket of the canister system, followed by partial lifting of the SNF loaded cask system out of the pool. The canister system is then dried using vacuum drying processes to remove the water inside the canister. No specific regulations or guidance exist prescribing specific procedure for the drying process. NUREG–1536 indicates that vacuum drying methods similar to the ones in PNL–6265 (NRC, 2010) are acceptable. Cask vendors have developed loading, draining, drying, and helium backfilling procedures specific to their canister to meet the maximum temperature of 400 °C for the clad under normal conditions (NRC, 2003) and the specified internal canister pressure of 3 torr after drying (NRC, 2010, Section 9.5.1). However, as indicated in ASTM C1553-16 and NUREG–1536, vendor recommended drying procedures may not be adequate in removing all free and bound water from the canister.

The drying process includes creating a vacuum level pressure in the canister cavity. The pressure is created by attaching one end of a tube through a narrow opening connected to canister cavity and attaching the other end of the tube to a vacuum pump which applies a suction force to the cavity. This creates a driving force for water to exit out of the canister cavity. In the process, the vacuum level pressure also results in lowering of vapor pressure in the cavity, leading to evaporation of liquid water. Sudden evaporation of liquid phase water could also result in formation of ice, i.e., solid phase water. Thus, water could exist in solid, liquid, and vapor phases in a canister cavity. Extent of either solid, liquid, or vapor water within the canister cavity is dependent upon momentum, heat, and mass transfers that occur during the drying process. Balancing the momentum, heat, and mass transfer operations during the drying process is complex and would require extensive resource expenses. However, recent work (Knight, 2018) has shown that formation of ice is likely during the drying process. Knight (2018) observed subzero temperatures in a mockup fuel assembly subjected to an industry practiced drying process. In addition, recent work (Bryan et al., 2019) by Sandia National Laboratory (SNL) under the high burnup cask demonstration project indicate presence of 100 g of residual water in a canister cavity. SNL work involved analyzing gas samples collected from an in-service canister loaded with SNF. Both works' (Knight, 2018; Bryan et al., 2019) results warrant an explanation for the presence of the residual water in the canister cavity. To this end, following qualitative analysis is presented.

During the vacuum drying process, as canister cavity pressure is lowered in sequential steps, water vapor pressure is also lowered. As water evaporates, i.e., liquid phase water converting into vapor phase water, internal energy balance must be satisfied. Latent heats of vaporization and melting of water are approximately 540 and 80 cal/g, respectively, at 1 atm. Although the latent heats are pressure and temperature dependents, the 1 atm values are used for the qualitative analysis. As liquid water evaporates, for each unit of liquid water evaporating into vapor phase, approximately 6 units of ice would form. Thus, as sequential pressure lowering steps are applied to the canister cavity, more and more liquid water converts to ice. In the vacuum drying steps, hold time between two pressure steps vary between 15 to 30 minutes. The hold times are set such that the ice formed during the pressure steps could be melted by decay heat of the fuel assemblies. However, heat transfer rate must be sufficiently high for the ice to melt during a pressure hold. Most of the ice is expected to accumulate at the bottom of the canister cavity. Radiative heat transfer between the fuel assemblies and the accumulated ice is expected to be negligible because of complex geometry which will result in near-zero view factor between the heat emitting fuel assemblies and the ice. Time constants associated with conductive heat transfer are

expected to range between a few minutes to several hours, not enough to melt all the ice between the pressure holds. Convective heat transfer is one potential mechanism that could lead to melting of ice during a hold time; but rate of convective heat transfer will be directly proportional to the density of cavity gas which will decrease with lowering of cavity pressure. Therefore, it is not certain that the ice formed during the vacuum drying process would be melted by the fuel assembly decay heats within the vacuum drying process timeframe.

This work assumes the presence of 5.5 and 10 moles of residual water in the canister cavity. The value of 5.5 moles is based on work by Bryan et al. (2019) in which residual free water at ~100 ml was reported in the HBU demonstration that used a typical vacuum drying process. The value of 10 moles is used considering uncertainties associated with logged water in failed rods and bound water with other assembly hardware (CNWRA, 2013; Bryan et al., 2019).

3.2 Fuel and Cladding Temperatures

The fuel and cladding temperatures are expected to vary in the storage space of the canister. If a canister is loaded with fuel assemblies with equal decay heat, the fuel and cladding temperature are expected to be maximum near center of a canister, otherwise, fuel and cladding temperature will be a complex function of each assembly decay heat and other related parameters. For the sake of simplicity, it is assumed that a storage canister is loaded with fuel assemblies with near equal decay heat, and maximum temperature occurs near the center of the canister. Recent work on modeling storage temperature of the high burnup fuel assemblies indicate peak temperature near 325 °C (Jensen and Richmond, 2019), however, there is no certainty that peak temperature will not be near 400 °C if utilities decide to store hotter fuel assemblies than the ones considered in Jensen and Richmond (2019). In addition, discussion with NRC staff indicated that the estimated peak temperature could have error of ±20 °C; therefore, it is assumed that zone peak cladding temperature is 400 °C for a limiting case, and 302 °C for a nominal case.

The fuel and cladding temperatures are expected to vary both temporarily and spatially. The temporal variations were modeled using an exponential decay function (McKinnon et al., 1992). The time-dependent fuel and cladding temperature $T(t)$ is given by the following equation

$$T(t) = (T_{init} - 309)\exp(-at) + 309 \qquad (3\text{–}1)$$

where T_{init} is the initial fuel and cladding temperature (K), and a is a thermal decay constant. The value of the decay constant (a) is either 0.023 or 0.064. A zone approach was used to model spatial variation of the fuel and cladding temperature; the approach is the same as the one used in CNWRA (2013). A short description is provided. Temperature distribution in a fuel basket loaded with 21 fuel assemblies with equal decay heats is presented in Figure 3–1; the distribution depiction is only for a quarter of the basket. As seen in the figure, the temperature varies spatially through the basket. The basket is divided into five temperature zones, as shown in Figure 3–2, to easily track the temperature distribution and its temporal variation. The fuel and cladding temperature in each zone is assigned a mean value, which is the average of the maximum and minimum temperatures in the zone. Various zone mean temperatures are listed in Table 3-1. The temporal variation in temperature in each zone is calculated using Eq. (3–1); T_{init} is replaced by mean value of the temperature in each zone denoted by T_{mean} and listed in Table 3-1.

Table 3-1. Mean Temperatures T_{mean} in Eq. (3–1) and Percentage of Volume of Five Temperature Zones

Zone Number	Fuel and cladding initial temperature K (°C) with peak temperature of 302 °C	Fuel and cladding initial temperature K (°C) with peak value of 400 °C	Percentage of total volume of fuel basket
1	575 (302)	673 (400.0)	18.95
2	525 (252)	623 (350.0)	33.00
3	475 (202)	573 (300.0)	33.72
4	425 (152)	523 (250.0)	12.38
5	375 (102)	481 (208.0)	1.95

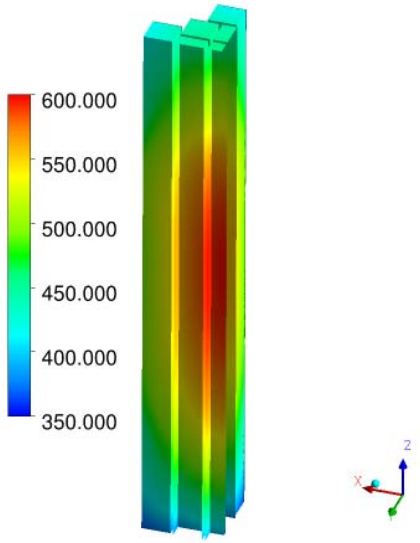

Figure 3–1. Temperature (K) Distribution in CASTOR V/21 Fuel Basket Assembly (CNWRA, 2013).

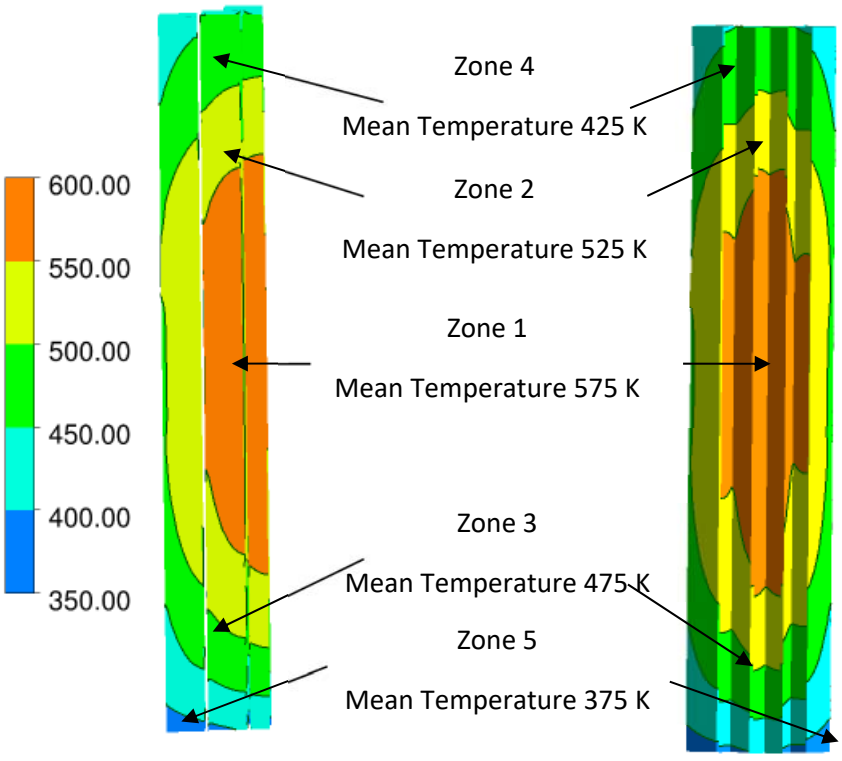

Figure 3–2. Location of the Five Temperature Zones in CASTOR V/21 Fuel Basket Assembly (CNWRA, 2013)

3.3 Radiolysis of Residual Water

Radiolysis of the residual water in the canister would generate various products, e.g., hydrogen and oxygen in accordance with following chemical reaction:

$$H_2O \leftrightarrow H_2 + \frac{1}{2}O_2 \tag{3–2}$$

Other radiolysis products such as hydrogen peroxide and various radicals are also generated via complex reaction paths described by Whitman and Hanson (2015).

Rate of decomposition of water molecules due to radiolysis is given by:

$$R_D = R_{ED} m_{water} G_{water} \tag{3–3}$$

where

R_D — Rate of decomposition of water molecules (molecules/sec)
R_{ED} — Rate of energy deposition in (eV/g/second)
m_{water} — Mass of a water (g)
G_{water} — G-value for water = 7.35 particles per 100 eV

Following the law of mass action, m_{water} can be expressed as

$$m_{water}(t) = m_0 exp\left(-\frac{R_{\mathrm{ED}} G_{\mathrm{w}} MW}{N_A} t\right) = m_0 exp\left(-\frac{t}{\tau}\right) \tag{3–4}$$

where t is time, m_0 is the initial amount of the residual water, MW is the molar mass of water, N_A is Avogadro's number, and time constant τ is defined as

$$\tau = \frac{N_A}{R_{ED} G_W MW} \tag{3–5}$$

Eq. (3–4) can be rewritten as

$$n_{water}(t) = n_0 exp\left(-\frac{t}{\tau}\right) \tag{3–6}$$

where $n_{water}(t)$ is the moles of water at a given instant, and n_0 is the initial moles of the water. Previous work (CNWRA, 2013) reported the radiation energy deposition rates in the range of 2.0×10^{14} and 3×10^{15} eV/g/s. The calculated values of time constants using Eq. (3-4) for deposition rates of 2.0×10^{14} and 3×10^{15} eV/g/s are 72.2 and 4.8 years, respectively. Previous work assumed that the radiation energy deposition rates are time-independent and uniform irrespective of water vapor location in a storage canister. It is noted that the rates would decrease with time as the total radiation level decreases in the canister. In addition, it is also noted that water recombination reactions, i.e., radiolysis products combining to form water and consumption of radiolysis products such as oxygen and hydrogen peroxide by fuel and cladding oxidation could drive the chemical reaction (3–1) equilibrium in either direction. Considering this, prior work assumed that 99.99% of the residual water gets decomposed in one time constant. As a result, water mole decomposition rate is given by

$$n_{water}(t) = n_0 exp(-1.929\, t) \tag{3–7}$$

for a time constant equal to 4.8 years, and

$$n_{water}(t) = n_0 exp(-0.129\ t) \tag{3–8}$$

for a time constant equal to 72.2 years.

Wittman and Hanson (2015) develop a comprehensive radiolysis model for water decomposition in a storage canister. The key model inputs included the dose rate induced by the radiation field in a storage canister. The authors compiled a list of gamma dose rates outside of pressurized water reactor (PWR) spent nuclear fuel rods as a function of age at a fixed temperature and relative humidity. It was assumed that the dose rate inside the canister equals gamma dose rate outside PWR SNF rod bundles. The estimated dose rate data were representative of a fuel bundle consisting of nine fuel assemblies, 4 wt% initial U-235 enrichment, 48 GW-day/MTU burnup, and 21-year decay time. Wittman and Hanson (2015) reported the following equation for the water decomposition:

$$m_{water}(t) = m_0 exp\left[-\frac{G_W MW}{N_A}\int_0^t \dot{d}(t)dt\right] \tag{3–9}$$

where

$$\begin{aligned}\dot{d}(t) = {} & 89.0967 \times exp[-0.0232748 \times (t + 12.134)] \\ & + 904.704 \times exp[-0.163135 \times (t + 12.134)] \\ & + 0.00825538 \times exp[-0.001 \times (t + 12.134)]\end{aligned} \tag{3–10}$$

Water mole fraction as a function of time computed using Eqs. (3–7),(3–8), and (3–9) are presented in Figure 3–3 (a). As seen in the figure, Wittman and Hanson (2015) model closely tracks the Eq. (3-7) results, indicating that the assumption of 99.9% decomposition in a time constant is reasonable. Recent work by Radulescu and Banerjee (2019) state that the dose rate in a high burnup storage canister could be several times higher than the low burnup storage canister. Raising the dose rate in Eq. (3–10) by a factor of 5 yielded water mole fraction similar to the one presented by red curve in Figure 3–3(b). This analysis justifies using Eq. (3–7) for water decomposition rate in storage canister loaded with high burnup SNF.

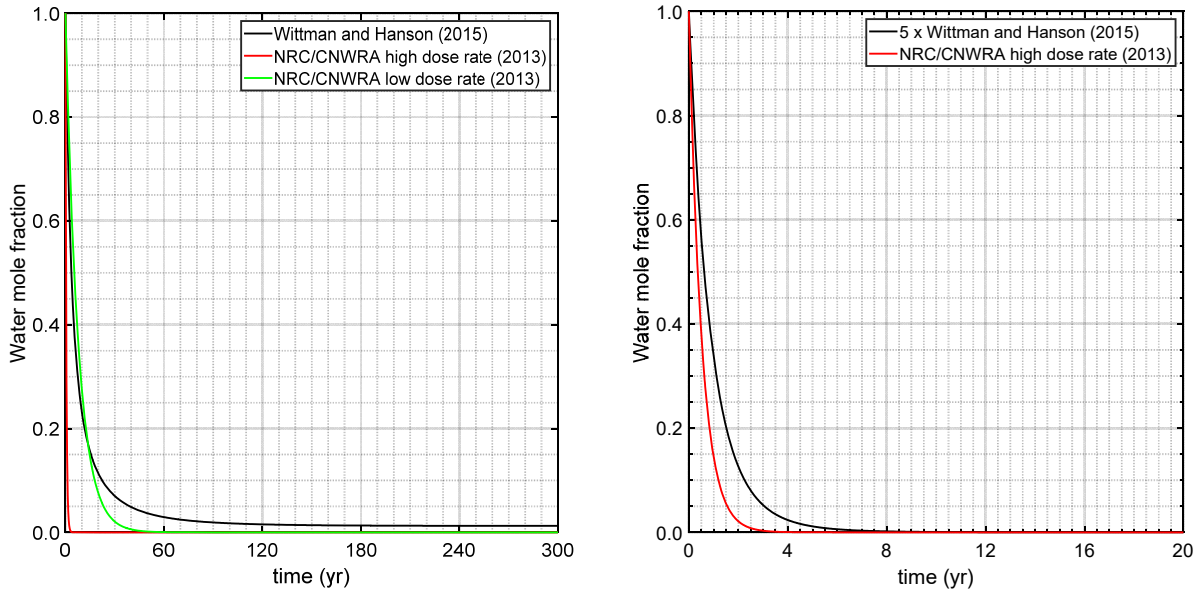

(a) **(b)**

Figure 3–3. Comparison of the Water Radiolysis Models

3.4 Cladding Oxidation Kinetics

There are two potential pathways for cladding oxidation due to residual water in dry storage: (i) cladding directly reacting with water molecules, (ii) water radiolysis products (i.e., oxygen and highly oxidizing species such as $OH^{\bullet}$ or H_2O_2) present in the canister can react with zirconium cladding to form zirconium oxide on the exposed cladding surfaces. Other environmental factors affecting cladding oxidation are relative humidity (RH) and temperature. Regarding (i), a direct reaction between water and zirconium would occur when water contacting the cladding material is either in the liquid phase or the RH is above a threshold value and the cladding temperature is sufficiently high (CNWRA, 2013). The threshold RH value is assumed to be 20 percent based on the similarity in thermodynamic and near equal nobility between zirconium and aluminum. For aluminum cladding, the minimum RH required to sustain detectable oxidation is approximately 20 percent at 150 °C. Because aluminum and zirconium have been shown to have a similar thermodynamic and practical nobility based on Pourbaix classification of the nobility order (Ghali, 2010) and exhibit a similar corrosion performance with the formation of a protective oxide film, a threshold RH of 20 percent can also be assumed for zirconium-based cladding materials. Regarding (ii), Suzuki and Kawasaki (1986) proposed following oxidation kinetics for Zircaloy-4 in air:

$$\Delta W\ (Zirc-4)\ = At\ \exp\ (-Q/\mathrm{R}T) \tag{3–11}$$

where

$\Delta W\ (Zirc-4)$	—	weight gain (g/m^2) for Zircaloy-4
A	—	preexponential constant ($g/m^2/hr$) = 3.25×10^5
t	—	time (hr)
Q	—	activation energy (J/mol) = 1.13×10^5
R	—	gas constant (J/mol/K) = 8.314
T	—	absolute temperature (K)

Oxidation rate data for ZIRLO™ and M5™ in the dry storage temperature range could not be found. Argonne National Laboratory (NUREG/CR-6846) conducted a study to estimate oxidation rates of steam-preoxidized Zircaloy-4, ZIRLO and M5 samples exposed to dry air at various temperatures. ANL rate constantans are applicable above 400 °C; the ANL data at and below 400 °C showed negligible mass gain in the samples exposed to the oxidation conditions. ANL used the data to estimate pre-exponential constant and *Q/R*; these two parameters are listed in Table 3-2. The rate constant estimated from the ANL data are for the oxidation growth phases of pre-breakaway and post-breakaway kinetics. Overall oxide growth phase can be divided in two periods: pre-breakaway and post-breakaway, as illustrated in Figure 3–4; initially a cyclic pre-breakaway period occurs in which initial parabolic growth is followed by kinetic transition into post-breakaway with accelerated corrosion and a new parabolic growth cycle. The rate constants for the pre-breakaway and post-breakaway oxide growth phases of Zircaloy-4, ZIRLO, and M5 are shown in Figure 3–5(a), Figure 3–5 (b), and Figure 3–5(c), respectively.

Oxidation rates for ZIRLO and M5 were estimated using the following expression

$$\Delta W\ (ZIRLO)\ = At\ \exp\ (-Q/\mathrm{R}T) \times \frac{k_{ZIRLO,ANL}}{k_{ZIRC-4,ANL}} \tag{3–12}$$

and

$$\Delta W\ (M5)\ = At \exp\left(-Q/\mathrm{R}T\right) \times \frac{k_{M5,ANL}}{k_{ZIRC-4,ANL}} \tag{3–13}$$

where

$\Delta W\ (ZIRLO)$ — weight gain (g/m^2) for ZIRLO
$\Delta W\ (M5)$ — weight gain (g/m^2) for M5
$k_{ZIRC-4,ANL}$ — Rate constant (kg^2/m^4/sec) for Zircaloy-4 based on ANL work
$k_{ZIRLO,ANL}$ — Rate constant (kg^2/m^4/sec) for ZIRLO based on ANL work
$k_{M5,ANL}$ — Rate constant (kg^2/m^4/sec) for M5 based on ANL work

It has been generally observed that the peak oxide thickness of Zircaloy-4 increased as the burnup increased up to approximately 75 GW-day/MTU (Garde, 1991; Van Swam, et al., 1997; EPRI, 2007); measurements of more than 4,400 commercial fuel rods irradiated in reactors worldwide show that the average oxide thickness on Zircaloy-4 was up to 100 μm for burnups in the range of 60–65 GW-day/MTU (EPRI, 2007). At low burnup (<45 GW-day/MTU), the average oxide thickness was 40 μm. Considering extent of oxidation of Zircaloy-4 during reactor operations and rate constants of pre- and post-breakaway phases, rate constant of the post-breakaway phase was used in Eqs. (3–12) and (3–13).

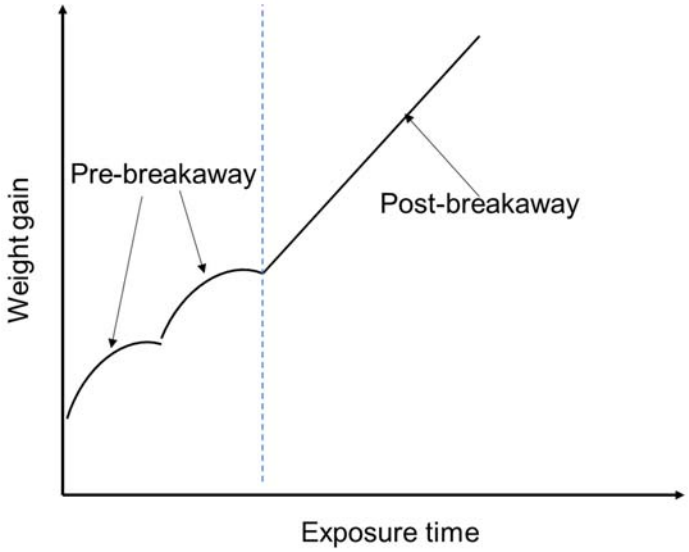

Figure 3–4. Schematic Representation of Pre-Breakaway and Post-Breakaway Oxide Growth Phases on Zr-Based Cladding Alloys

Compared to Zircaloy-4 cladding, oxidation data for new alloys are still lacking to confirm the range of oxide thickness at the high burnup regime (Cheng et al., 2000). However, for ZIRLO rods having an average burnup of 52.5 GW-day/MTU, the average peak oxide thickness for ZIRLO was 31 μm, which is approximately 27.5 percent of the average oxide thickness for conventional Zircaloy-4 (Sabol, et al., 1994). Considering that ZIRLO oxidation extent is smaller than Zircaloy-4, but the oxidation regime in dry storage is likely to be post-breakaway, post-breakaway rate constant values in Eq. (3–12) were used.

Data for M5 indicate that the oxide layer thickness is expected to range between 10 to 30 μm in 30 to 55 GW-day/MTU burnup range (Mardon et al, 2010). The pre-breakaway rate constant for M5 is an order of magnitude higher than the post-breakaway constant below 400 °C, as in Figure 3–5 (c). Considering that oxide growth during dry storage is expected to be post-breakaway phase, the post-breakaway rate constant values in Eq. (3–13) were used. Zircaloy-4 rate constant from Suzuki and Kawasaki (1986), and ZIRLO and M5 rate constants in Eqs. (3–12) and (3–13), respectively, are presented in Figure 3–6.

Table 3-2. Values of Preexponential Constant and Ratio of Activation Energy to Gas Constant for Zircaloy-4, ZIRLO, and M5			
Cladding alloy	**Oxide growth phase**	**Preexponential constant *A* ($kg^2/m^4/sec$)**	**Ratio of activation energy and gas constant *Q/ R* (K)**
Zircaloy-4	Pre-breakaway	0.386	16070
	Post-breakaway	187.3	19245
ZIRLO	Pre-breakaway	0.86	16100
	Post-breakaway	1.72×10^4	22865
M5	Pre-breakaway	1.0×10^{-3}	12230
	Post-breakaway	1.3×10^5	25290

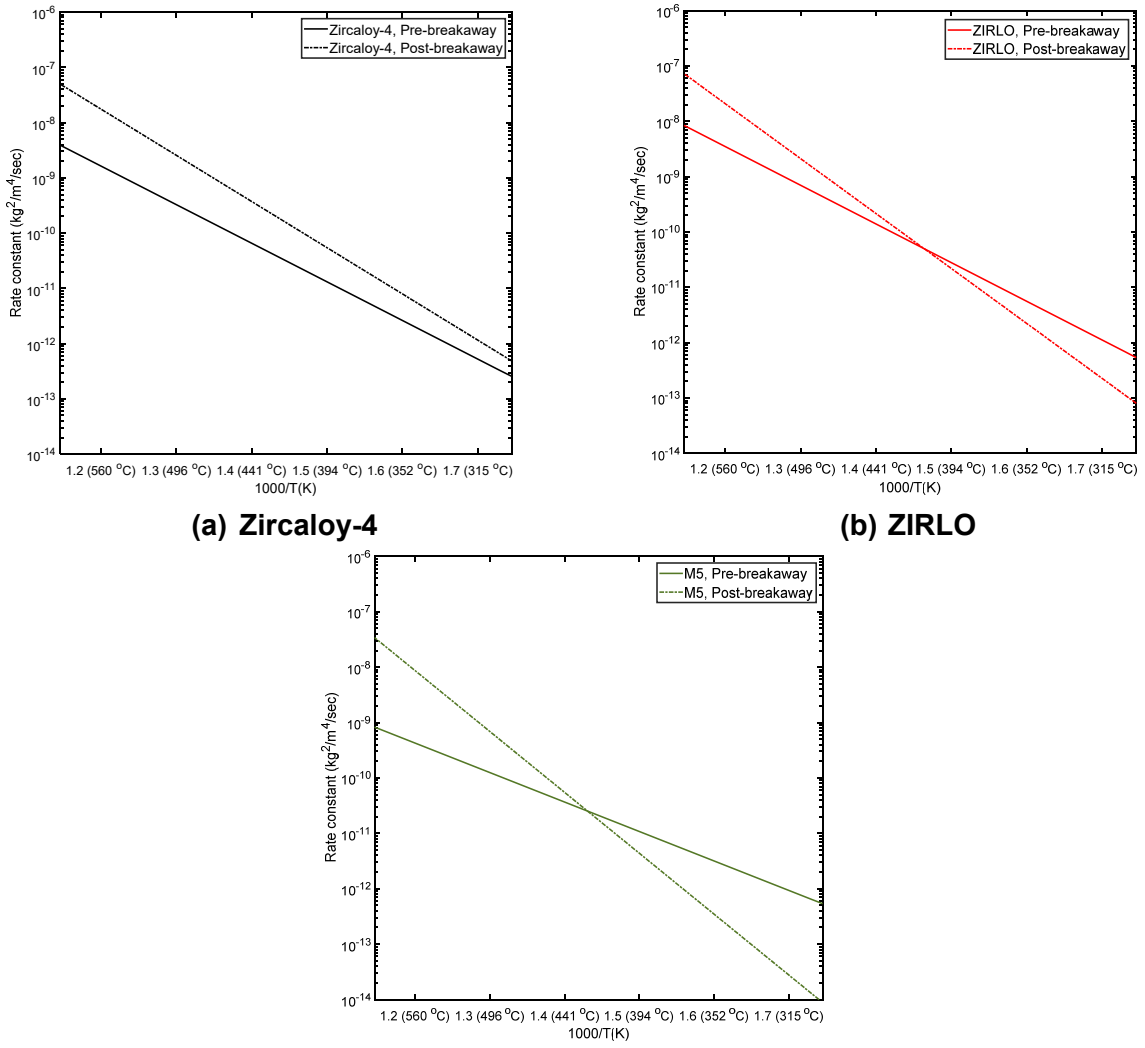

Figure 3–5. Rate Constant as a Function of Temperature for (a) Zircaloy-4, (b) ZIRLO, and (c) M5 in Temperature Range of 300 to 600 °C

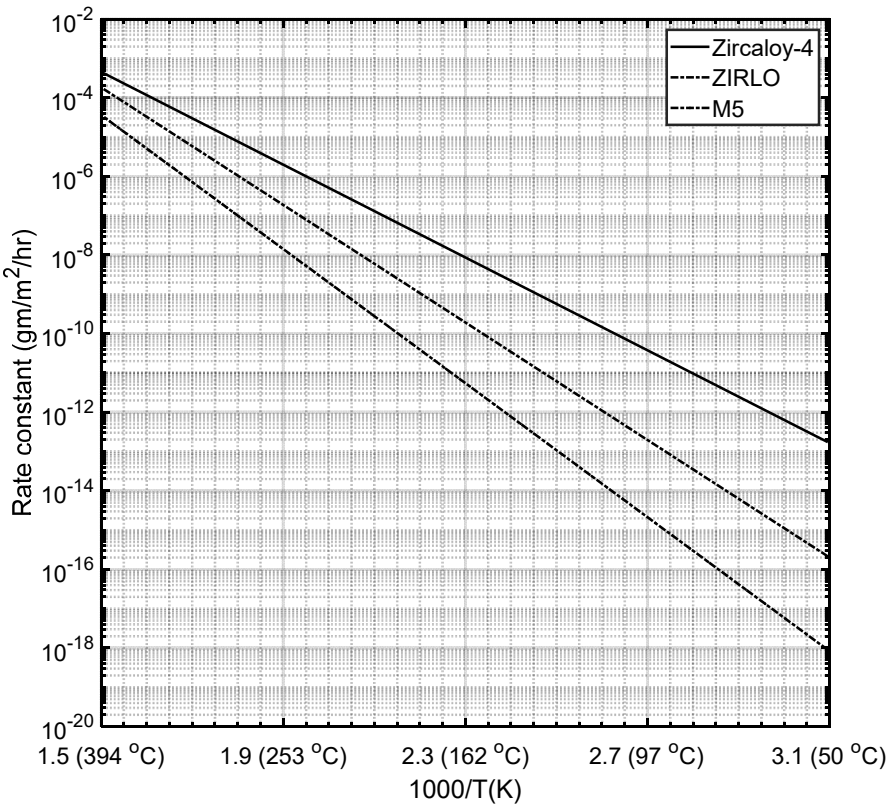

Figure 3–6. Rate Constant versus Temperature for Zircaloy-4, ZIRLO, and M5 in Dry Storage Temperature Range

3.5 Fuel Oxidation Kinetics

Irradiated UO_2 fuel can react with oxidants such as oxygen, water vapor, or other oxidizing radiolytic products. UO_2 could be oxidized to form U_4O_9, U_3O_7, and U_3O_8 in dry air with RH less than 40 percent or could also form hydrated uranium oxides, such as schoepite ($UO_3 \cdot xH_2O$, x = 0.5 to 2) in humid air RH greater than 40 percent of RH) or an aqueous environment (Ahn, 1996; Einziger, et al., 1992; Einziger and Strain, 1986; Einziger and Cook, 1985; EPRI, 1986; McEachern and Taylor, 1998; Taylor, et al., 1995; Wasywich, et al., 1993).

Irradiated LWR SNFs with typical burnup of 20 to 50 GW-day/MTU have been shown to oxidize via the two-step reaction in air as in Eq. (3–11) (Hanson, 1998; Einziger, et al., 1992; Thomas, et al., 1989; Thomas, et al., 1993)

$$UO_2 \rightarrow U_4O_9 \rightarrow U_3O_8 \tag{3–14}$$

LWR SNF is first oxidized by formation of nonstoichiometric U_4O_9 preferentially along the grain boundaries to reach an oxygen-to-metal (O/M) ratio of approximately 2.4 (often denoted as U_4O_{9+x} or $UO_{2.4}$). Grain boundary openings due to presence of fission gas at the grain boundaries in the LWR SNF may facilitate oxygen diffusion (Einziger, et al., 1992; Thomas, et al., 1989). $UO_{2.4}$ then further oxidized to U_3O_8 without producing intermediate phase such as U_3O_7 (Hanson, 1998; Thomas, et al., 1993). For Canada Deuterium Uranium (CANDU) SNF, two oxidation models were observed: a grain model and a fragment model (Wasywich, et al., 1993). In a fragment model, the oxidation was occurred along the fracture-free surface of the fragments and expanded to the UO_2 grains. However, at high RH, the CANDU fuel was oxidized by preferential diffusion of oxygen along the grain boundaries.

The extent of fuel oxidation in a storage canister can be correlated with two controlling parameters: kinetics of the SNF oxidation and availability of oxidants (oxygen and water vapor) present in the canister. For example, if the kinetics is slow and oxidant is abundant, kinetics can control the overall reaction. However, for the opposite case (i.e., fast kinetics and limited amount of oxidant), the overall reaction will be controlled by the rate of the radiolysis process and consumption rate of oxidant with time. Important factors that affect the UO_2 oxidation and hydration include temperature, RH, and SNF burnup. Effects of these factors on fuel oxidation are discussed next.

3.5.1 Temperature

Temperature strongly affects the fuel oxidation rate. Below 230 °C in a dry air environment, $UO_{2.4}$ is generally observed in LWR SNF because the kinetics of U_3O_8 formation is believed to be too slow to be detected on a reasonable laboratory time scale (McEachern and Taylor, 1998; Thomas, et al., 1993). The time for conversion of UO_2 into $UO_{2.4}$ has been shown to have Arrhenius dependence with temperature in accordance with following equation (Einziger, et al., 1992; Ahn, 1996)

$$t_{2.4}(\text{yr}) = 2.97 \times 10^{-13} \exp\left(\frac{26.6 \text{ kcal/mole}}{RT}\right) \tag{3–15}$$

Assuming oxygen diffusion through a layer of $UO_{2.4}$ from the individual grain surface to inside the grain to be the rate-controlling step, the growth kinetics of the oxidized width as per the following equation (Einziger, et al., 1992)

$$w\ (\mu\text{m}) = (2kt)^{0.5} \tag{3–16}$$

where

t — oxidation time (hr)
k — rate constant (μm^2/hr)

The rate constant measured in the temperature range of 175 to 195 °C is given by

$$k\left(\frac{\mu m^2}{hr}\right) = 1.04 \times 10^8 \exp\left(\frac{\text{-24.0 kcal/mole}}{RT}\right) \quad (3\text{–}17)$$

Equations (3–15) to (3–17) were developed using the weight gain measurement tests of the LWR SNF to reach an O/M ratio of near 2.4 when individual grains oxidized close to 100 percent of U_4O_9.

Above 230 °C, as observed by Einziger and Cook (1985), U_3O_8 could be a primary oxide phase. The formation of U_3O_8 has been shown to follow a nucleation-and-growth mechanism and displays a sigmoidal trend for reaction kinetics (McEachern and Taylor, 1998). The incubation time is defined as the time for full conversion of $UO_{2.4}$ plus the time required for enough U_3O_8 to form. The incubation time can be estimated by the following equation (Einziger and Strain, 1986; Stout and Leider, 1994; Ahn, 1996)

$$t_{U3O8}(\text{yr}) = 1.56 \times 10^{-19} \exp\left(\frac{44.1 \text{ kcal/mole}}{RT}\right) \quad (3\text{–}18)$$

The calculated times for complete conversion from UO_2 to $UO_{2.4}$ and from UO_2 to U_3O_8 as functions of temperature using Eqs. (3–15) and (3–18), respectively, are presented in Figure 3–7. The conversion time data decreases exponentially with increasing temperature. Note that the time for conversion to U_3O_8 could be valid only above 230 °C because U_3O_8 was not observed below 230 °C when experiments were conducted in dry air. Below 230 °C, $UO_{2.4}$ was normally observed as a primary phase in dry air oxidation at RH below 40 percent. Table 3-3 lists calculated times required to convert to $UO_{2.4}$ or U_3O_8 at various temperatures at and above 230 °C. The conversion time is relatively short at temperatures above 250 °C. In addition, changes in the storage temperature are expected to occur slowly. A time derivative of Eq. (3–1) yields:

$$\frac{dT(t)}{dt} = -a(T_{mean} - 309)\exp(-at) \quad (3\text{–}19)$$

The temperature decay rate as a function of time is presented in Figure 3–8 for a equal to 0.023 and 0.064. As seen in the figure, the decay rate is more for a equal to 0.064 than 0.023. The temperature decay rates around 250 °C for a equal to 0.023 and 0.064 are approximately equal to 4.5 and 17 °C/yr; these temperature decay rates are sufficiently small for the fuel to stay near a temperature value sufficiently long for it to get oxidized till completion. Additional literature search indicated that 250 °C is temperature above which formation of U_3O_8 occurs concurrently and measurable rate (McEachern and Taylor, 1998; Kang et al, 2007; Kim et al.,1997) for the low burnup fuel. Considering totality of the literature information, fuel and cladding temperature and temperature decay rate, 250 °C is used as threshold temperature above which low burnup fuel will get oxidized to U_3O_8, otherwise, fuel oxidation will result in formation of $UO_{2.4}$.

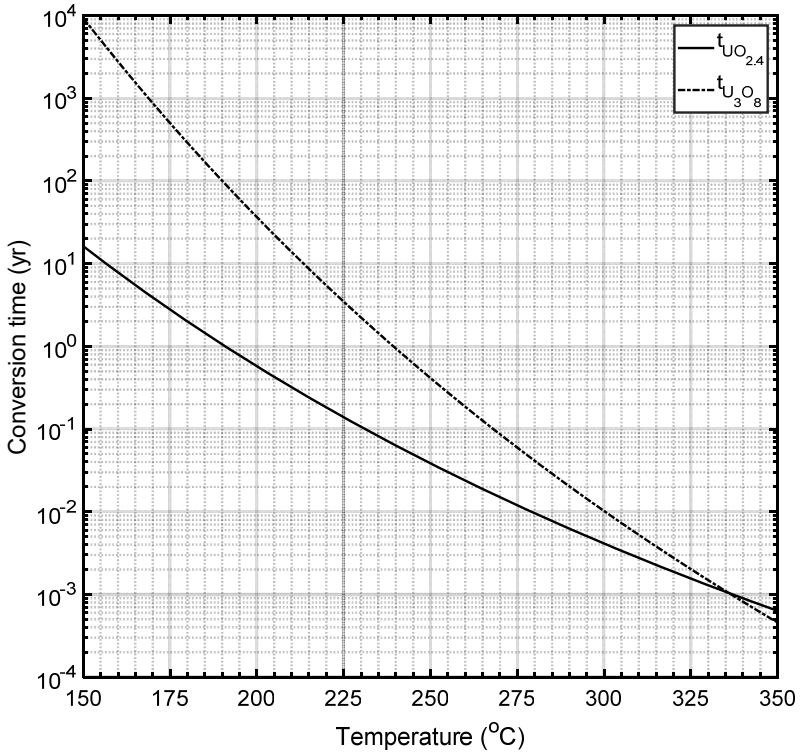

Figure 3–7. Conversion Time of UO_2 to $UO_{2.4}$ and UO_2 to U_3O_8 as a Function of Temperature

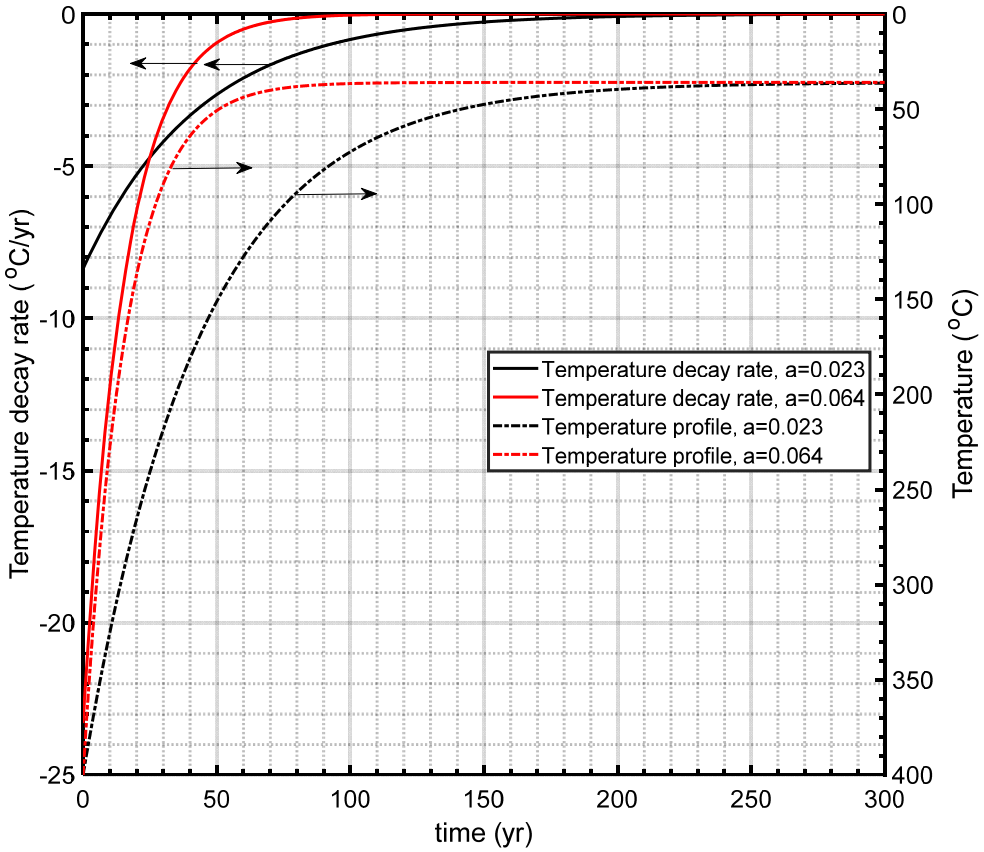

Figure 3–8. Evolution of Peak Fuel and Cladding Temperature and Temperature Decay Rates

Table 3-3. UO_2 to $UO_{2.4}$ and UO_2 to U_3O_8 Conversion Times at Various Temperatures				
Temperature (°C)	**UO_2 to $UO_{2.4}$ conversion time (yr)**	**UO_2 to U_3O_8 conversion time (yr)**	$\frac{t_{U3O8}(yr)}{t_{2.4}(yr)}$	$t_{U3O8} - t_{2.4}(yr)[days]$
230	0.11	2.23	20.96	2.12 [774]
235	0.08	1.44	17.65	1.36 [493]
240	0.06	0.94	14.91	0.88 [321]
245	0.05	0.62	12.63	0.57 [208]
250	0.04	0.41	10.73	0.37 [135]
275	0.01	0.06	4.98	0.05 [18]
300	4.10×10^{-3}	1.02×10^{-3}	2.47	6.1×10^{-3} [2.2]
335	1.07×10^{-3}	1.10×10^{-3}	1.02	2.3×10^{-3} [0.84]

3.5.2 Relative Humidity

Relative humidity, i.e., moisture can affect UO_2 oxidation and hydration. Presence of sufficient moisture under sufficient high temperature can lead to formation of compounds such as UO_3-H_2O hydrates. Moisture can also enhance the extent of grain boundary oxidation, as compared with dry air oxidation (Taylor, et al., 1995; Wasywich, et al., 1993; McEachern and Taylor, 1998). The degree or effect of moisture was dependent on the moisture content (i.e., RH).

According to Taylor, et al. (1995), at RH below 40 percent, UO_2 oxidation products were same as for the case of dry air oxidation (e.g., U_3O_7/U_4O_9 or U_3O_8). The experiments Taylor, et al. (1995) conducted involved using un-irradiated UO_2 in an autoclave under controlled RH and temperature ranging from 200 to 225 °C. At RH above 40 percent, the unirradiated UO_2 oxidation resulted in a mixture of U_3O_8 and dehydrated schoepite ($UO_3 \bullet 0.8H_2O$).

3.5.3 Fuel Burnup

Fuel burnup may affect the oxidation behavior of SNF as the structure and chemistry of the fuel can change with burnup level. It is observed that SNF is more porous with more grain boundary openings and fission products with increasing burnup. Einziger, et al. (1992) previously showed no clear correlation of burnup with oxidation rate of UO_2 to $UO_{2.4}$ in a burnup range of 27 to 48 GW-day/MTU in temperature range of 175 to 195 °C. At high temperature, however, Hanson (1998) reported an incubation time increase for a full conversion to $UO_{2.4}$ with increasing burnup of LWR fragments tested at 305 °C. The incubation time increased from about 10 hours to 100 hours for 16 and 42 GW-day/MTU, respectively. Hanson (1998) suggested possible retardation effect of substitutional cations, such as uranium to plutonium, and fission products delay or hinder U_3O_8 formation. Herranz and Feria (2009) presented a similar dependence of the incubation time on the burnup for CANDU and LWR fuels (8 to 27 GW-day/MTU). The higher burnup delayed U_3O_8 formation at the temperature of 200 to 400 °C. Einziger and Strain (1986) reported an increase in the time required for spallation with powdered U_3O_8 formation, with increased burnup (22.1 to 26.7 GW-day/MTU) at 295 °C for PWR fragments. Kansa et al. (1998) proposed following correlation for U_4O_9-to-U_3O_8 transition activation energy:

$$E_A = E_{A0} + \alpha B \tag{3–20}$$

where

E_A — U_4O_9-to-U_3O_8 transition activation energy (kcal/mole)

E_{A0} — Zero burnup activation energy = 37 kcal/mole
α — Coefficient for burnup dependence, nominally = 0.287 kJ/mole per GW-day/MTU
B — Burnup (GW-day/MTU)

and expression for the rate constant is given by

$$k_{U3O8} = k^0_{U3O8} \times exp\left(-\frac{E_A}{RT}\right) \quad (3\text{–}21)$$

where $k^0_{U3O8}$is the pre-exponential constant.

As per activation energy-burnup correlation in Eq. (3–20), the rate constant in Eq. (3–21) decrease with increasing burnup. Ratio of rate constants for high burnup and low burnup fuels as a function of temperature are presented in Figure 3–9. As seen in the figure, the ratio decreases with increasing burnup for a given temperature, and the ratio increases with increasing temperature for a fixed burnup. The figure data also indicate that a higher temperature limit is needed for all UO_2 converting to U_3O_8, like the 250 °C for the low burnup fuel. An analysis is conducted to determine temperature value when $UO_{2.4}$ will convert to U_3O_8 in relatively short period. Based on t_{U3O8}, $t_{2.4}$, and rate constants given by Eqs. (3–15), (3–18), (3–21), respectively, the following expression is proposed to determine the temperature limits:

$$(t_{U3O8} - t_{2.4}) \times exp\left(\frac{E_A(x) - E_A(40)}{RT}\right) = 0.37 \quad (3\text{–}22)$$

where *x* is the burnup for which temperature limit is to be determined. Eq. (3–22) was solved for various values of burnups. A plot of burnup versus temperature determined by Eq. (3–22) is presented in Figure 3–10. The transition temperature values in Figure 3–10 for burnups of 45, 50, 55, and 62 GW-day/MTU are 266, 282, 297, and 315 °C.

An additional complexity arises with the formation of rim layer structure with the high burnup fuel above the burnup of 45 GW-day/MTU. The rim layer structure is normally observed on the outmost surface of the LWR fuels. The rim structure has unique microstructure and chemistry characteristics compared to that of the fuel body in the center. The rim layer is represented by submicron grain size, high porosity with many micropores, and high concentrations of actinides and fission gases (Manzel and Walker, 2002; Rondinella and Wiss, 2010; Bruno and Ewing, 2006). However, rim layer effects are not considered in the fuel oxidation kinetics.

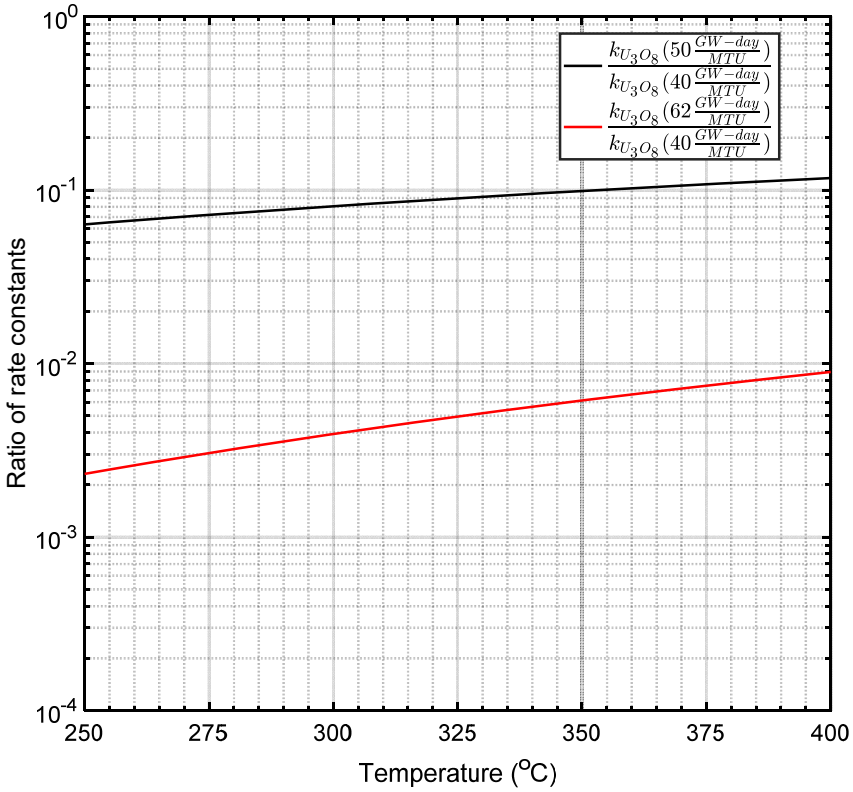

Figure 3–9. Ratio of $UO_{2.4}$-to-U_3O_8 Transition Rate Constants

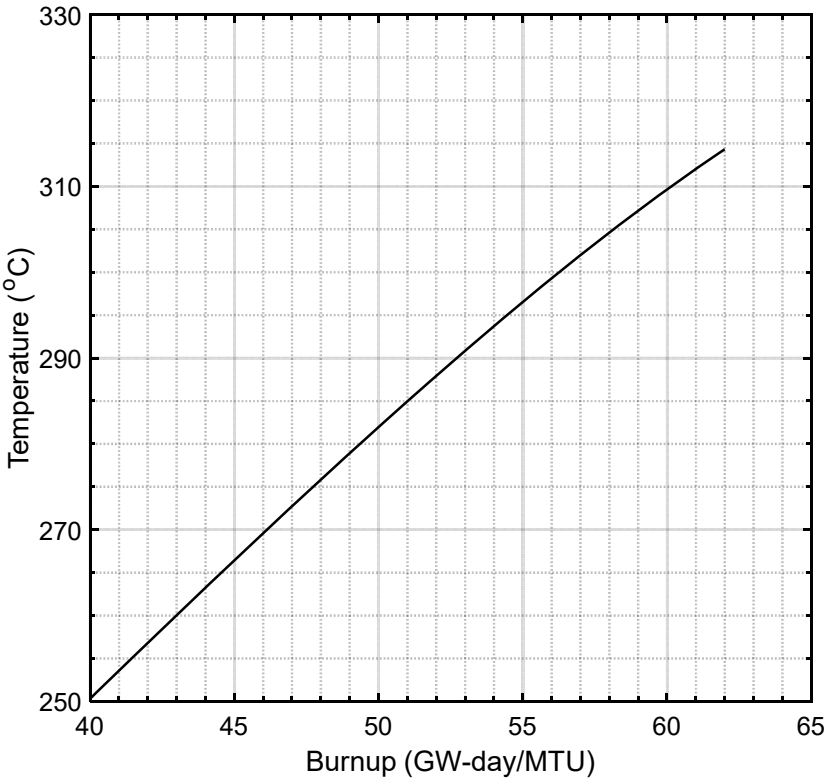

Figure 3–10. Burnup versus $UO_{2.4}$-U_3O_8 Transition Temperature

3.5.4 Fuel Oxidation Model

As discussed previously, oxidation or hydration behavior of SNF can depend on the temperature and RH in terms of reaction kinetics and formation of the oxide phase. To delineate the effect of temperature and RH on fuel oxidation and hydration in the canister environment, the following three temperature ranges are defined: $T \geq T^*$ where T^* is burnup dependent, $150 \leq T < T^*$, and $T < 150$ °C. Above T^*, the primary oxidized phase will be U_3O_8 irrespective of the RH, and the oxidized fuel can be assumed to be fully converted to U_3O_8 once $UO_{2.4}$ forms considering relatively short conversion times at high temperature as listed in Table 3-3. UO2 to UO2.4 and UO2 to U3O8 Conversion Times at Various TemperaturesWhen temperature ranges between $150 < T < T^*$, the UO_{2+x} primary oxidized phase is $UO_{2.4}$ independent of RH in the fuel oxidation model. Below 150 °C, $UO_{2.4}$ is the primary phase when RH <40 percent, while schoepite ($UO_3 \cdot xH_2O$) is the oxidized phase when RH >40 percent. Table 3-4 summarizes the fuel oxidation model along with the applicable kinetic equations.

Table 3-4. Criteria for Temperature and Relative Humidity for Fuel Oxidation Kinetics Used in Partitioning of Residual Water

Temperature and Relative Humidity	Oxide phase	Applicable kinetics and justification
$T \geq T^*$ (independent of RH) T^* determined from Figure 3–10 data; =250, 266, 282, 297, and 315 °C for 40, 45, 50, 55, and 62 GW-day/MTU, respectively	U_3O_8	$UO_{2.4}$, $w = (2kt)^{0.5}$ is used as all UO_2 fully converts to U_3O_8 above T^*
$150 \leq T < T^*$ (Independent of RH)	$UO_{2.4}$	$w = (2kt)^{0.5}$
$T < 150$ (RH < 40%)	$UO_{2.4}$	$w = (2kt)^{0.5}$
$T < 150$ (RH ≥ 40%)	$UO_3 \cdot xH_2O$ ($x < 2$)	Schoepite and similar hydrates can forms. Dissolution rate data in NUREG–1914 (NRC, 2008) is used to estimate the conversion rate. NUREG–1914 data indicate that rate from 0.01 to 6.85 $mg/m^2/day$.

3.6 Integration Model

An integration model was used to quantitatively estimate extent of cladding and fuel oxidation that could occur due to residual water in the canister. The model is the same as the one used in the CNWRA study. The model was reconstructed using the code listing available in NRC (2014).

The model accounts for both temporal and spatial variation of temperature and RH and their effects on cladding and fuel oxidation. The model integrated the radiolysis of residual water, fuel and cladding oxidation, temperature distribution.

The model consists of inputs, outputs, and calculations. Model inputs, the calculation method, and model outputs are described in the next three subsections. The model assumptions, wherever applicable, are also defined.

3.6.1 Model Inputs

The model inputs include cask parameters, fuel temperature at the time of loading, residual water amount, cask internal volume, number of fuel assemblies, fuel rods per fuel assembly, dimensions of each fuel rod and fuel pellet, number of fragments per pellets, size of each grain in a fuel pellet, density of various UO_{2+x} phases, and void fraction in each fuel pellet. Because the fuel and cladding temperatures are expected to vary spatially, the canister inside the cask volume is divided into five zones as detailed in Section 3.2. The inputs also include the radiolysis rate of water over the assumed storage time of 300 years. In each zone, it is assumed that the fuel and cladding temperatures are uniform. It is also assumed that the fuel temperature asymptotically approach to ambient in 300 years. Initial fuel and cladding temperatures and volume fraction of each zone are input to the model. A fraction of failed cladding percentage is also input. This fraction is used to calculate the number of exposed fuel pellets available for oxidation. For example, a failed cladding fraction of 0.1 percent amounts to failure of 1 fuel rod out of 1,000. The failed rod is assumed to have a crack of a certain length that is specified in the model. Various cladding, fuel, and canister model input parameters are listed in Table 3-5; the listed parameters are obtained from various sources including Kesterson et al. (2013).

Table 3-5. Cladding, Fuel, and Canister Parameter Values Used in the Integration Model

Parameter	Values
Canister void volume	2.1 m^3
Number of fuel assemblies	21
Fuel rods per assembly	208 in 15 × 15 Babcock & Wilcox Fuel Assembly
Fuel rod length	3.9 m
Fuel rod outer diameter	10.92 mm
Pellet diameter	9.36 mm
Pellet length	15.24 mm
Axial length of a crack on a failed rod	3.5 cm
Fuel pellet void volume	5%
UO_2 density	10.96 g/cm^3
$UO_{2.4}$ density	11.30 g/cm^3
U_3O_8 density	8.35 g/cm^3
$UO_3 \cdot xH_2O$* (x <2) density	4.89 g/cm^3
UO_2 grain shape	spherical
UO_2 grain radius	10 μm
Volume fraction Zones 1, 2, 3, 4, and 5	19, 33, 33.7, 12.4, and 1.9%, respectively
ZrO_2 density	5.6 g/cm^3
* x is assumed to be zero in the integration model.	

The cladding failure rates of 0.1 is used in the model. This value is based upon the literature information on cladding failure rate data available in literature. The physical condition of the fuel rods and assemblies at the time they are placed into dry storage is virtually unchanged from when they are removed from the reactor because degradation during storage in the spent fuel pool is minimal (CRWMS M&O, 2000). Some fuel rods can have initial defects, such as manufacturing micro defects, handling-induced defects including small partial depth cladding wall cracks, weld defects, moisture or organic contamination of cladding or pellets, and excessive gaps at spacers that permit vibration and fretting. During reactor operations, cladding can fail by pellet-cladding interactions, stress corrosion cracking, and debris-induced fretting.

Data from studies of Zircaloy-based cladding failure rates from 1968 to 1973 indicate that 1 in 100 fuel rods had cladding failures (CRWMS M&O, 2000; Locke, 1974). A later study reported that the overall

cladding failure rate had decreased to 0.36 percent for BWR and 0.04 percent for PWR fuel rods as a result of design and material performance improvements (Cohen & Associates, 1999). From the measurement of Kr-85 leaking from approximately 26,500 rods currently in dry storage, the overall observed failure rate is estimated to be 0.045 percent (CRWMS M&O, 2000). Considering this literature information, 0.1 percent cladding failure rate was used in the model.

3.6.2 Calculation Sequence

In the initial step, storage time is divided into several timesteps. Before conducting sequential calculations as a function of time, the following calculations are conducted.

- Cladding surface areas in each zone are estimated based upon volume fraction in each zone. Cladding surface areas are estimated by multiplying the zone volume fraction by the total surface area of the cladding. The number of fuel rods in each zone is also estimated by multiplying the zone volume fraction with total rods in a canister.

- The number of failed fuel rods in each zone is estimated by multiplying the number of fuel rods in each zone with the failure rate, which is the same as the failure rate of the cladding. The model inputs include cladding failure rates of 0.1 percent, and 4,368 fuel rods. The cladding failure rate of 0.1 percent yield four failed rods. It is assumed that there is one failed rod in each of the hotter zones (i.e., Zones 1–4) for the 0.1 percent failure rate.

- The number of affected fuel pellets exposed to the canister environment due to failed cladding in a zone is estimated. Literature information (Einziger and Cook, 1985) indicates that the affected fuel pellets with a crack of a specified length in a fuel rod include pellets located 3 cm on either side of the crack as well as all pellets directly underneath the axial length of the crack. Thus, effective crack length for fuel oxidation is equal to the dimension of the crack along the length of the fuel rod plus 6 cm. A schematic diagram depicting a crack oriented axially along a fuel rod is presented in Figure 3–11. As seen in the figure, the effective crack length for fuel oxidation exceeds the crack length. The number of affected fuel pellets in a zone is calculated using Eq. (3–23).

$$N_{pellets\_zone} = floor\left(\frac{\text{effective crack length}}{\text{pellet length}} \times \text{number of failed fuel rods in a zone}\right) \qquad (3\text{–}23)$$

where $N_{pellets\_zone}$ denotes the number of affected pellets in a zone. The *floor* function in Eq. (3–23) rounds the calculated number within the parentheses down to the lowest integer.

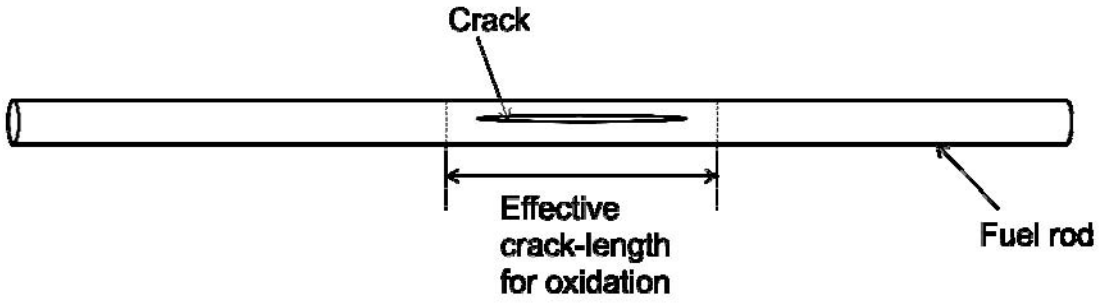

Figure 3–11. Schematic Representation of a Crack Oriented Along the Length of the Fuel Rod. The Effective Crack-Length for Fuel Oxidation is Equal to Crack Length Plus 6 cm.

- Literature information (Einziger and Cook, 1985) also indicates fuel pellets directly underneath a crack tend to be oxidized sooner than fuel pellets not directly exposed but underneath the effective crack length for oxidation. Considering this, it is assumed that the fuel pellets directly underneath the crack undergo oxidation before the other fuel pellets. It is also assumed that the oxidation of the other pellets begins only after the directly exposed fuel pellets have been completely oxidized. The number of directly exposed fuel pellets in a zone is determined by Eq. (3–24)

$$N_{directly-exposed\_pellets\_zone} = floor\left(\frac{\text{crack length}}{\text{pellet length}} \times \text{number of failed fuel rods in a zone}\right) \quad (3\text{–}24)$$

where $N_{directly-exposed\_pellets\_zone}$ denotes the number of directly exposed fuel pellets in a zone. The number of other fuel pellets in a zone is calculated by subtracting the number of directly exposed fuel pellets from the number of affected fuel pellets.

- The exposed area for fuel oxidation is also estimated. A fuel pellet is expected to fragment into 10–30 pieces during the reactor operation. It is assumed that the fuel fragments in 16 pieces, as shown in Figure 3–12. The surface area for fuel oxidation per pellet is calculated by determining the number of grains per pellet and then multiplying it with the surface area of each grain. The number of grains per pellet is calculated by Eq. (3–25)

$$N_{grains\_per\_pellet} = floor\left[\frac{V_{pellet} \times (1 - f_{void})}{V_{grain}}\right] \quad (3\text{–}25)$$

where

$N_{\text{grains}\_per\_pellet}$ — number of grains per pellet
V_{pellet} — volume of a pellet
V_{grain} — volume of a grain
f_{void} — void volume fraction in a pellet

The corresponding surface area per pellet for fuel oxidation for the first mechanism is calculated by Eq. (3–26)

$$A_{oxidation\_per\_pellet\_fm} = N_{grains\_per\_pellet} \times A_{grain} \quad (3\text{–}26)$$

where

$A_{oxidation\_per\_pellet\_fm}$ — surface area for fuel oxidation per pellet for the first mechanism
A_{grain} — surface area of each grain

- The temperature of each zone is calculated as a function of time.

- It is implicitly assumed that the fuel and cladding temperatures are not affected by the amount of residual water. The fuel and cladding temperatures are assumed to vary with time according to Eq. (3–27). The justification for using the equation is detailed in Section 3.2.

$$T_{fuel\_cladding\_zone} = (T_{mean} - T_{ambient})exp(-at) + T_{ambient} \quad (3\text{–}27)$$

where

$T_{fuel\_cladding\_zone}$ — temperature of fuel and cladding in a zone
T_{mean} — mean value of initial temperature in a zone at the time of fuel loading
$T_{ambient}$ — ambient temperature, 309 K
a — thermal decay constant

- Before marching in time, the RH in each zone is also calculated at the time of loading and at the first timestep. It is assumed that the water is distributed in each zone according to the following equation

$$n_{water\_zone} = n_{water} \times f_{zone} \quad (3\text{–}28)$$

where

n_{water_zone} — moles of water in a zone
n_{water} — moles of water in the canister
f_{zone} — volume fraction of a zone

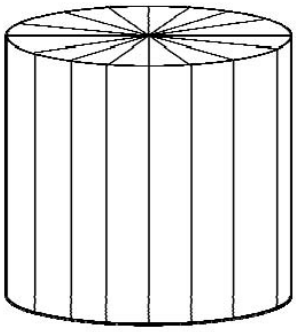

Figure 3–12. Schematic Representation of a Cylindrical Fuel Pellet Fragmented into Sixteen Pieces

The partial pressure of water in each zone is calculated using the ideal gas law, and RH is calculated by dividing the partial pressure with the saturated pressures. The calculations are marched in time. The following calculations are conducted at each timestep.

(1) The amount of oxygen produced due to radiolysis between the two timesteps is calculated. The fuel and cladding temperatures between the two timesteps in a zone are assumed to be equal to the average of the temperatures at the two timesteps. Similarly, RH in a zone between the two timesteps in a zone is assumed to be equal to the average of the relative humidities at the two timesteps.

(2) The amount of oxygen consumed by the fuel pellets and cladding between the two timesteps using the rate models in each zone is calculated. If the total oxygen produced by radiolysis is more than the oxygen consumed by fuel and cladding oxidation in all the zones, the calculations are continued to the next timestep. However, if the total oxygen consumed by fuel and cladding oxidation in all the zones is more than the oxygen generated by the radiolysis, the radiolysis-controlled fuel and cladding oxidation model is applied. This is explained next.

(3) In the radiolysis-controlled oxidation model, the amount of oxygen fuel and cladding oxidation consume in Zone 5, the coldest zone, is estimated. If the moles of oxygen

generated due to radiolysis in Zone 5 are less than the amount needed for fuel and cladding oxidation, the amount of oxygen generated between the two timesteps is divided between the fuel and cladding according to Eqs. (3–29) and (3–30)

$$n_{oxygen\_fuel\_oxidation\_zone\_5} = \left(\frac{A_{exposed\_fuel\_zone\_5}}{A_{exposed\_fuel\_zone\_5} + A_{clad\_zone\_5}}\right) \times n_{oxygen\_generated\_\_zone\_5} \quad (3–29)$$

$$n_{oxygen\_clad\_oxidation\_zone\_5} = \left(\frac{A_{clad\_zone\_5}}{A_{exposed\_fuel\_zone\_5} + A_{clad\_zone\_5}}\right) \times n_{oxygen\_generated\_zone\_5} \quad (3–30)$$

where

$n_{oxygen\_fuel\_oxidation\_zone\_5}$	—	moles of oxygen consumed by fuel oxidation in Zone 5
$n_{oxygen\_clad\_oxidation\_zone\_5}$	—	moles of oxygen consumed by cladding oxidation in Zone 5
$n_{oxygen\_generated\_zone\_5}$	—	moles of oxygen generated between two timesteps in Zone 5
$A_{exposed\_fuel\_zone\_5}$	—	surface area of the exposed fuel in Zone 5
$A_{clad\_zone\_5}$	—	surface area of cladding in Zone 5

However, if the moles of oxygen generated due to radiolysis in Zone 5 are greater than the oxygen needed for fuel and cladding oxidation, the leftover oxygen in Zone 5 is calculated according to Eq. (3–31)

$$n_{oxygen\_leftover\_zone\_5} = n_{oxygen\_generated\_zone\_5} - n_{oxygen\_fuel\_oxidation\_zone\_5} - n_{oxygen\_clad\_oxidation\_zone\_5} \quad (3–31)$$

where $n_{oxygen\_leftover\_zone\_5}$ denotes moles of oxygen not consumed by cladding and fuel oxidation in Zone 5. These moles of oxygen are added to the moles of oxygen generated in Zone 4. Thus, the effective moles of oxygen present in Zone 4 between the two timesteps are equal to the one in Eq. (3–32)

$$n_{oxygen\_present\_zone\_4} = n_{oxygen\_generated\_zone\_4} + n_{oxygen\_leftover\_zone\_5} \quad (3–32)$$

where

$n_{oxygen\_present\_zone\_4}$	—	moles of oxygen present in Zone 4 for fuel and cladding oxidation
$n_{oxygen\_generated\_zone\_4}$	—	moles of oxygen generated by radiolysis in Zone 4 between two timesteps

Again, the moles of oxygen consumed by fuel and cladding oxidation in Zone 4 are calculated. If the moles of oxygen present in Zone 4 are less than the amount needed for

fuel and cladding oxidation, the moles of oxygen are partitioned between the cladding and fuel according to Eqs. (3–33) and (3–34)

$$n_{oxygen\_fuel\_oxidation\_zone\_4} = \left(\frac{A_{exposed\_fuel\_zone\_4}}{A_{exposed\_fuel\_zone\_4} + A_{clad\_zone\_4}}\right) \times n_{oxygen\_present\_zone\_4} \quad (3\text{–}33)$$

$$n_{oxygen\_clad\_oxidation\_zone\_4} = \left(\frac{A_{clad\_zone\_4}}{A_{exposed\_fuel\_zone\_4} + A_{clad\_zone\_4}}\right) \times n_{oxygen\_present\_zone\_4} \quad (3\text{–}34)$$

where

$n_{oxygen\_fuel\_oxidation\_zone\_4}$	—	moles of oxygen consumed by fuel oxidation in Zone 4
$n_{oxygen\_clad\_oxidation\_zone\_4}$	—	moles of oxygen consumed by cladding oxidation in Zone 4
$A_{exposed\_fuel\_zone\_4}$	—	surface area of the exposed fuel in Zone 4
$A_{clad\_zone\_4}$	—	surface area of cladding in Zone 4

Otherwise, the excess moles of oxygen are transferred to Zone 3. This process is repeated for the remaining three zones.

(4) A counter is used to keep track of the moles of oxygen produced by radiolysis and consumed by cladding and fuel oxidation throughout the preceding timesteps. If the moles of oxygen produced by radiolysis reach a plateau, and the difference between moles of oxygen produced by radiolysis and the total moles of oxygen consumed by fuel and cladding oxidation is less than a specified tolerance limit, calculations are stopped.

(5) When the criterion to stop the calculations is not met, a computational check is conducted to determine whether the directly exposed fuel pellets in a zone have been completely oxidized. If the directly exposed fuel pellets have been completely oxidized in a zone, the other fuel pellets undergo oxidation in the next timestep. A computational check is also conducted to determine whether the affected fuel pellets (i.e., the directly exposed and other fuel pellets) have been completely oxidized in a zone. If the affected fuel pellets have been completely oxidized, only cladding oxidation is implemented in the next timestep.

(6) Steps 1–5 are repeated until the net oxygen production criterion is met and the calculations are stopped.

3.6.3 Model Outputs

The integrated model calculates the extent of fuel and cladding oxidation, and the moles of oxygen consumed by both fuel and cladding in each zone. The model also calculates fuel and cladding temperatures; RH; and the moles of oxygen, hydrogen, and water in the canister as a function of time.

3.7 Cladding Failure Criterion

3.7.1 Threshold Strain for Cladding Rupture

Oxidation of UO_2 to U_3O_8 can generate stress on cladding as U_3O_8 swells (36 percent when 100 percent conversion to U_3O_8). Volume expansion occurs due to less dense structure of U_3O_8 with density of 8.35 g/cm^3 compared to that of UO_2 with density of 10.96 g/cm^3, with fluorite structure of UO_2 transitioning to the orthorhombic structure of U_3O_8 (Taylor, et al., 1989). Volume expansion of an oxidized fuel pellet can split the cladding and propagate the crack once the strain reaches the threshold value of 6.5 percent of strain at the defected area on the LWR fuel rod (Einziger and Cook, 1985). Einziger and Cook (1985) reported X-ray diffraction analysis of the oxidized fuel samples revealed that only U_3O_8 was observed for the case of the highest dilation area at the defect present on the fuel rod. The experiments were conducted at approximately 230 °C in air and for a hole size of 0.76 mm. The cladding was observed to have crack lengths of 11.3 mm after 2,235 hours of exposure, and 55.1 mm after 5,962 exposure hours. The authors also reported that volume expansion of 5.1 percent was correlated with approximately 25 percent conversion of UO_2 to U_3O_8. In addition, Einziger and Cook (1985) reported that a strain of 2 percent correlated with approximately 50 percent conversion.

An analysis was conducted to estimate cladding strain as a function of UO_2 pellet conversion to U_3O_8. The analysis included estimating initial pellet mass and volume based on density of UO_2, mass of oxidized pellet and volume based on densities of UO_2 and U_3O_8, and change in radius of pellet as a function of conversion. The cladding wall thickness was assumed to be 600 μm for the analysis. The analysis accounted for void volume of the pellet and interspace between fuel pellet and cladding inner diameter. It was assumed that increase in volume of the pellet resulted in diametric increase of the pellet in accordance with following equation:

$$\frac{(d^2 - d_0^2)}{d_0^2} = \frac{\Delta V}{V} \tag{3–35}$$

where

d — diameter of the oxidized fuel pellet (mm)
d_0 — diameter of the initial UO2 pellet (mm)
$\frac{\Delta V}{V}$ — fractional change in volume due to fuel oxidation

Parameters associated with pellet dimensions, UO_2 and U_3O_8 densities, and cladding dimensions are listed in Table 3-5. The data from the analysis is listed in Table 3-6.

Table 3-6. Volume and Radius Increases for Various Values of Conversion Fraction to U_3O_8

Conversion Fraction of UO_2 to U_3O_8	Mass of Oxidized Fuel Pellet (g)	Volume of Oxidized Fuel Pellet (mm^3)	Percentage Change in Volume	Diameter of the Oxidized Pellet (mm)	Diametric Strain on Cladding (%)
0.05	10.94	1013.78	1.76	9.20	NA*
0.10	10.96	1031.41	3.53	9.28	NA*
0.15	10.98	1049.10	5.31	9.36	NA*
0.20	11.00	1066.85	7.09	9.44	NA*
0.25	11.03	1084.67	8.88	9.52	NA*
0.30	11.05	1102.54	10.67	9.60	NA*
0.35	11.07	1120.48	12.47	9.68	NA*
0.40	11.09	1138.48	14.28	9.75	0.34
0.45	11.11	1156.54	16.09	9.83	1.13
0.50	11.13	1174.66	17.91	9.91	1.92

Table 3-6. Volume and Radius Increases for Various Values of Conversion Fraction to U_3O_8

Conversion Fraction of UO_2 to U_3O_8	Mass of Oxidized Fuel Pellet (g)	Volume of Oxidized Fuel Pellet (mm^3)	Percentage Change in Volume	Diameter of the Oxidized Pellet (mm)	Diametric Strain on Cladding (%)
0.55	11.16	1192.85	19.74	9.98	2.70
0.60	11.18	1211.09	21.57	10.06	3.49
0.65	11.20	1229.40	23.41	10.13	4.27
0.70	11.22	1247.77	25.25	10.21	5.04
0.75	11.24	1266.19	27.10	10.29	5.81
0.80	11.26	1284.69	28.96	10.36	6.58
0.85	11.29	1303.24	30.82	10.43	7.35
0.90	11.31	1321.85	32.69	10.51	8.12
0.95	11.33	1340.53	34.56	10.58	8.88
1.00	11.35	1359.27	36.44	10.66	9.63
NA*: cladding inner diameter is 9.72 mm based on outer diameter of 10.92 mm and wall thickness of 600 μm, no strain occurs till oxidized fuel pellet diameter exceeds cladding inner diameter.					

As listed, 100 percent conversion to U_3O_8, increase in pellet diameter can exert up to 9.63 percent strain, and 6.5 percent strain limit, reported by Einziger and Cook (1985), occurs at approximately 80 percent conversion. Einziger and Cook (1985) also reported that strains associated with conversion to 20 and 50 percent were estimated to be about 1 and 2 percent, respectively, whereas strain of 1.91percent is achieved at 50 percent conversion as per the listed data in Table 3-6. Fuel swelling during reactor operation and storage is assumed to be negligible in developing the analysis data listed in Table 3-6.

Some of the potential reasons for differences between the listed data in Table 3-6 and Einziger and Cook (1985) are likely to be due to following reasons:

- It is assumed that fuel pellet porosity is 5 percent (Bailey and Tokar, 1982) which accommodates fuel expansion until approximately 15 percent conversion. Porosity of the irradiated fuel could differ from the initial porosity. A lower porosity value will result in higher strain on the cladding for a given value of conversion.

- The analysis does not consider the intermediate phase of $UO_{2.4}$ whose density (11.30 g/cm^3) is slightly higher than that of UO_2 density (10.96 g/cm^3), leading to a volume reduction (~2 percent) when oxidized from UO_2 to $UO_{2.4}$ (BSC, 2004).

- Other features present in the irradiated fuel, such as cracks and grain boundary openings with burnup, can also dissipate stresses.

Other relevant data is also discussed. Hastings, et al. (1985) reported that that 15 percent conversion to U_3O_8 was enough to produce the 2 percent diametrical increase required to split the cladding. Novak, et al. (1983) reported about 2 percent strain was necessary for initiation of crack growth on the used CANDU fuel. When compared to the 6.5 percent strain in Einziger and Cook (1985), the CANDU fuel threshold is quite low and could be due to the lower burnups of CANDU fuel compared to LWR SNF, resulting in different structure and chemistry of the CANDU SNF compared to the LWR SNF. In this work 80 percent conversion criterion corresponding to approximately 6.5 percent strain in Table 3-6 is used to determine risk of cladding gross rupture.

3.7.2 Fracture Toughness Criterion for Flaw Extension

A fracture mechanics approach was also developed to estimate threshold cladding strain for gross rupture. The approach is described next. The cladding deformation due to uniform pellet oxidation and swelling is approximated by an axisymmetric condition. Under this simplification, the cladding hoop strain ($\varepsilon_{\theta\theta}$) is expressed as:

$$\varepsilon_{\theta\theta} = \Delta R/R \tag{3–36}$$

where R is the cladding mean radius and ΔR is the amount of average cladding expansion. Instead of solving a full elastic solution, a simple, uniaxial Hooke's law is used to calculate the hoop stress ($\sigma_{\theta\theta}$) in the cladding with the Young's modulus (modulus of elasticity) E:

$$\sigma_{\theta\theta} = E\varepsilon_{\theta\theta} \tag{3–37}$$

By Linear Elastic Fracture Mechanics (LEFM), the opening mode (Mode I) stress intensity factor (K_I) of a crack in the cladding longitudinal (axial) direction is given by

$$K_I = \sigma\sqrt{\pi a}\cdot F(\lambda) \tag{3–38}$$

where a is the half crack length, σ is the tensile stress to open the crack ($\sigma = \sigma_{\theta\theta}$ in the present case), $\lambda = a/\sqrt{Rt}$, t is the cladding thickness, and the geometric-dependent function $F(\lambda)$ is

$$F(\lambda) = \sqrt{1 + 1.25\lambda^2},\ \text{for } 0 < \lambda \leq 1 \tag{3–39}$$

and

$$F(\lambda) = 0.6 + 0.9\lambda,\ \text{for } 1 \leq \lambda \leq 5 \tag{3–40}$$

Note that the above solution (Tada et al, 1985) is similar to the formula proposed by Structural INTegrity Assessment Procedures (SINTAP) for European Industry (Laham, 1998). The companion solution (Tada et al, 1985) for the crack opening area is given as

$$A = \frac{\sigma}{E}2\pi Rt\cdot G(\lambda) \tag{3–41}$$

with

$$G(\lambda) = \lambda^2 + 0.625\lambda^4 \text{for } 0 < \lambda \leq 1 \tag{3–42}$$

and

$$G(\lambda) = 0.14 + 0.36\lambda^2 + 0.72\lambda^3 + 0.405\lambda^4,\ \text{for } 1 \leq \lambda \leq 5 \tag{3–43}$$

By assuming that the deformed crack takes the form of an ellipse (Chu, 2014), the equivalent crack opening displacement ($2b$) can be calculated by equating the crack opening area (A) to the area of an ellipse, that is, πab, where the crack length $2a$ is the major axis of the ellipse and $2b$ is its minor axis. For the calculation of stress intensity factor and crack opening area, only cladding thickness (typically 0.6 mm) and its Young's modulus are needed. The Young's modulus in this analysis is selected to be 100 GPa for high burn-up fuel cladding. However, to estimate the critical values of cladding hoop strain (ΔR/R), crack opening area, and crack opening displacement (above which values the crack will become unstable and unzip the fuel rod), the cladding fracture toughness (K_{IC}) must be experimentally obtained. Note that the fracture toughness of high burn-up cladding, denoted by K_{IC} or K_q {K_q was defined on the basis of the first detectable onset of crack growth or load drop in fracture testing (Raynaud et al., 2007)},

has not been fully characterized, but the experimental procedure using Spiral Notch Torsion Test (SNTT) technology has been established and can be easily implemented for in-cell testing (Wang, 2019). In this current exploratory investigation, two K_{IC} values (25 and 90 MPa√m) (Raynaud et al., 2007; Sindelar et al., 2011) are used to bound the analysis results. It should be noticed that K_{IC} is sensitive to hydride orientation.

Figure 3–13, Figure 3–14, and Figure 3–15 show the estimated critical values of crack length, crack opening area, and crack opening displacement, respectively, as a function of cladding hoop strain.

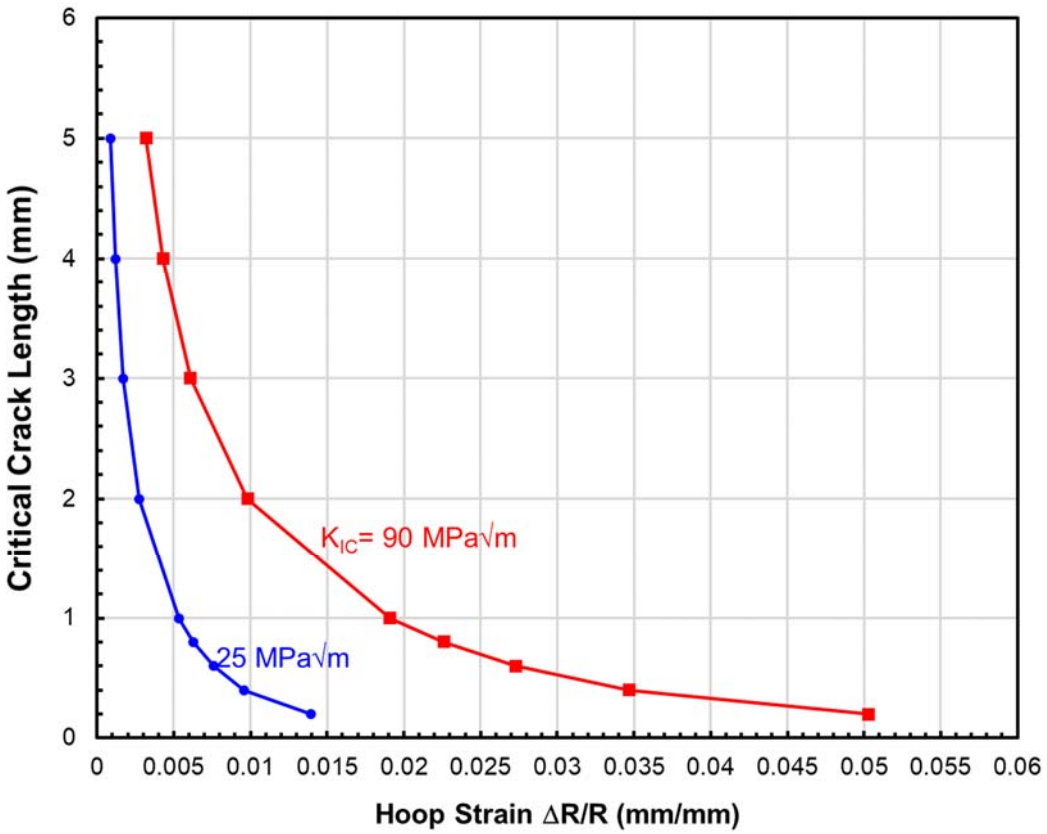

Figure 3–13. Critical Crack Length versus Cladding Hoop Strain

3.7.3 Crack Growth Rate

The following evaluation is for a condition of unlimited available oxygen in the canister such as would be assumed for a failed canister that would have allowed air ingress.

Cladding defects such as pinholes and through-wall hairline crack cladding can grow when the exposed fuel is oxidized to form more U_3O_8 near the defect. EPRI (1986) estimated crack growth rates for LWR SNFs in burnup range of 8 to 38 GW-day/MTU burnup with defects of 8 to 760 μm long. The crack initiated at the defects propagated mainly in the axial direction along the fuel rod. The crack growth rates ranged from 3×10^{-4} to 2.3×10^{-3} cm/min in temperature range of 250 to 360 °C. The strain required for crack propagation was estimated to be 6.5 percent for the 760 μm defect, and the threshold strain was estimated to be less than 1 percent for the defect sizes ranging from 8 to 37 μm. A reason for lower strain for the lower crack sizes is not apparent.

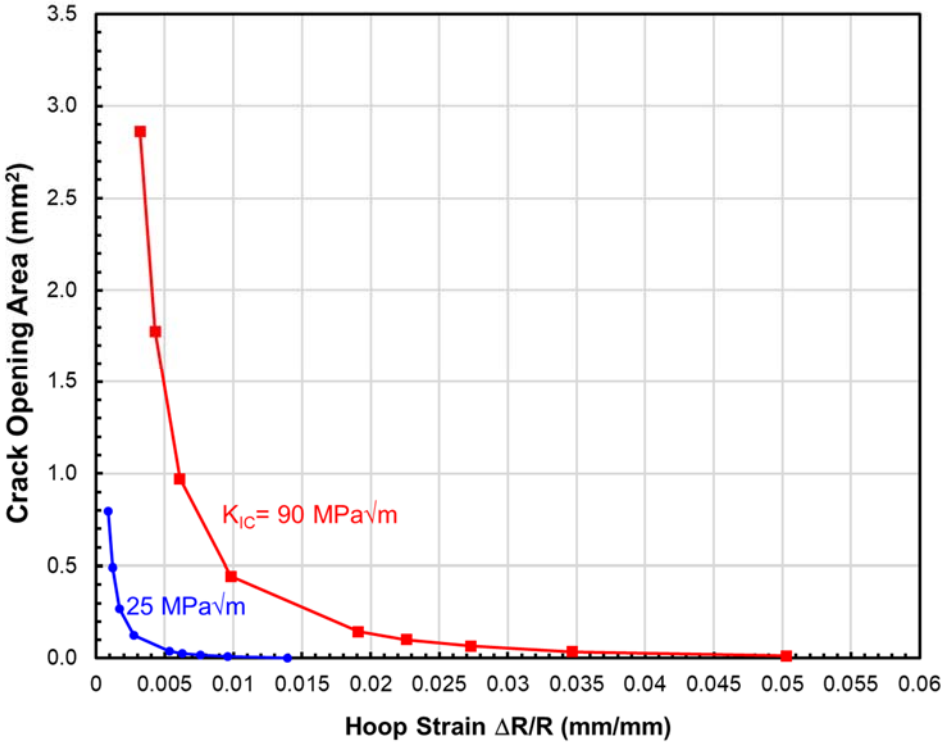

Figure 3–14. Crack Opening Area versus Cladding Hoop Strain

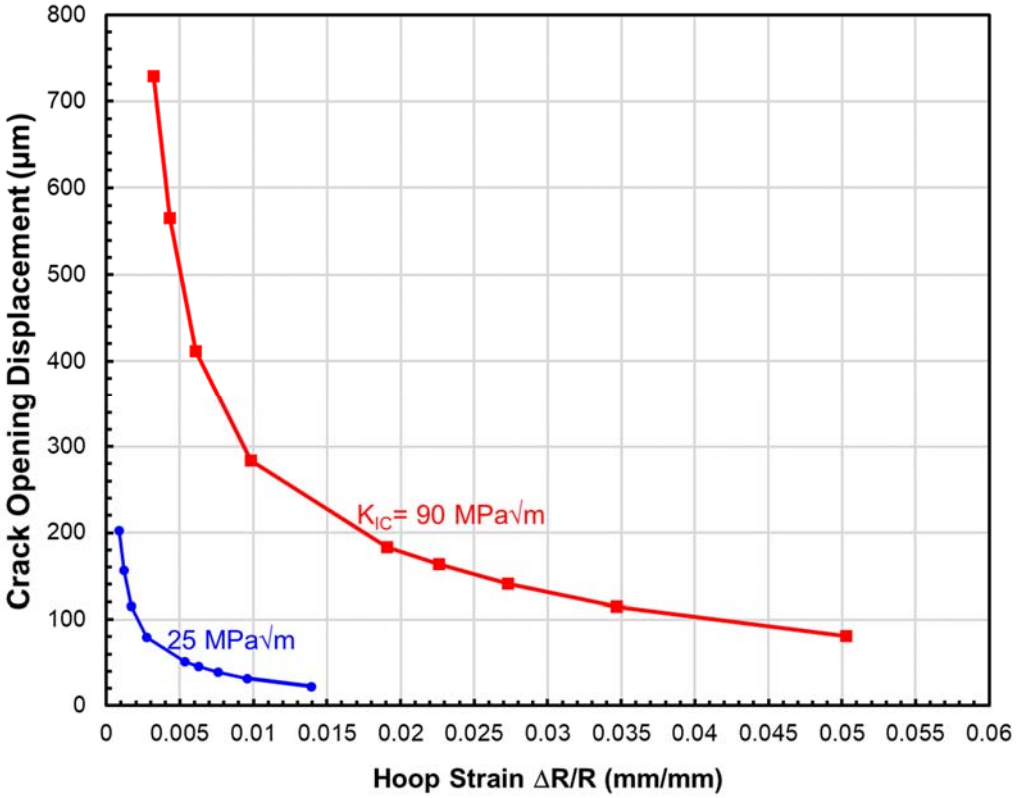

Figure 3–15. Crack Opening Displacement versus Cladding Hoop Strain

BSC (2007) proposed following equation for crack propagation rate, i.e., crack growth velocity:

$$V_{cp} = V_0 \, exp\left(-\frac{E_{cp}}{RT}\right) \tag{3–44}$$

where

V_{cp} — Crack propagation rate (cm/min)
V_0 — coefficient = 4.98×10^6 cm/min
E_{cp} — Activation energy associated with crack propagation = 104.8 kJ/mole

The calculated crack growth velocity according to Eq. (3–44) is presented in Figure 3–16(a). The growth velocity as a function of time for both high- and low-end temperature conditions are presented in Figure 3–**16**(b) and Figure 3–16(c) . The crack growth rate data in Figure 3–16(a) is used to estimate time required to grow a 10 cm long crack at different temperatures. The data is listed in Table 3-7. The listed data show that the time required to grow a 10-cm long crack is relatively short; for example, it takes only 41 days for a 10 cm long crack to form if fuel underneath has oxidized at 250 °C. The time required to form the 10cm long crack decrease with increasing temperature. Thus, if enough oxygen is available to form U_3O_8, fuel oxidation can continue to the maximum extent possible without being inhibited by the crack opening. However, this scenario is not analyzed in the integration model.

Table 3-7. Time Required to Form 10-cm Long Axial Crack at Various Temperatures

Temperature (°C)	Time Required (days) to Form 10−cm Long Axial Crack
250	41
275	14
300	5
325	2
350	1
375	0.4

Gross rupture of a cladding is defined when crack width exceeds 1 mm (NRC, 2007). Kohli, et al. (1985) reported that the initial crack size of the damaged LWR fuel ranged from 0.4 to 7 cm with average length of 3.5 cm. After 2,100 hours' exposure in the air at 325 °C, the crack propagated up to about 10 cm in the axial direction. Einziger and Cook (1985) have reported a crack width increase for the initial defect size of the 0.76-mm hole on the BWR SNF. With oxidation of the fuel rods in air at 229 °C, the rods were breached at the defect sites and the crack width from the two different locations of the holes increased either 1.37 mm in width and 1.128 cm in length after 2,235 hours, and 4.55 mm in width and 5.51 cm in length after 5,962 hours. The area affected by formation of U_3O_8 near the defect was estimated to be approximately ± 3 cm in the axial direction when tested at 229 °C after 5,962 hours' exposure in air. Once the fuel rod splits at a defect due to fuel swelling, cracks can propagate quickly at high temperatures due to rapid continued increase in fuel oxidation kinetics (if oxidizing conditions exist).

This crack growth rate kinetics section was included in this report to provide insights to fuel behavior for the postulated condition of high, unlimited oxygen (e.g. air environment) in a canister. It is not applicable for the postulated condition of residual water in an intact canister that is the focus of this report.

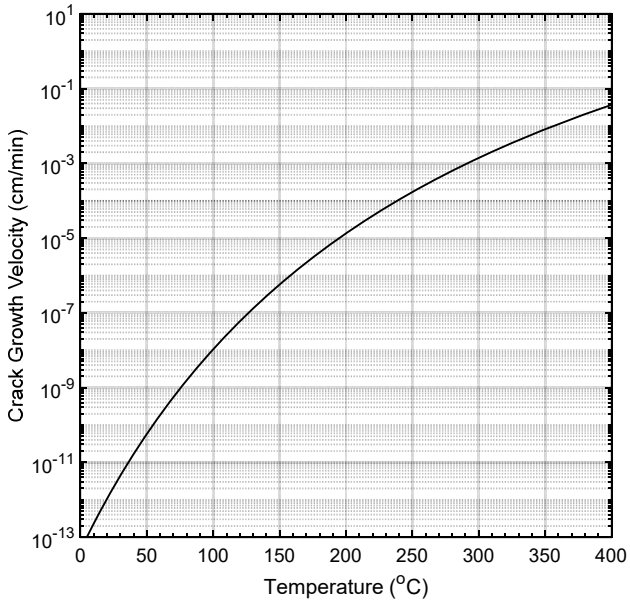

(a) Crack Growth Velocity with Temperature

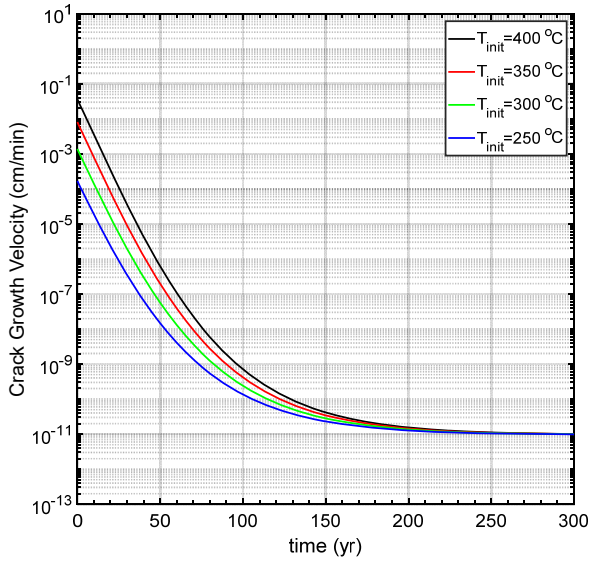

(b) Crack Growth Velocity with Time for High-End Temperature Condition

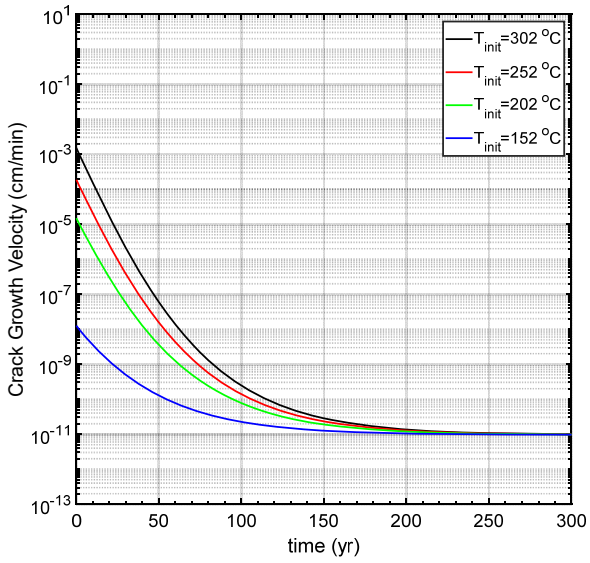

(c) Crack Growth Velocity with Time for High-End Temperature Condition

Figure 3–16. (a) Crack Growth Velocity with Temperature, and Crack Growth Velocity with Time for (b) High-End, and (c) Low-End Temperature Conditions

4. SIMULATION DATA AND RESULTS: Splitting of Residual Water Between Fuel and Cladding

The integration model was run for various combinations of the parameters listed in Table 4-1 to evaluate several cases. These cases, which are listed in Table 4-2, correspond to various parametric uncertainties and their combinations.

Table 4-1. List of Varying Parameters and Their Values in the Integrated Model

Parameter	Value
Fuel and cladding initial temperature	Low- or high-end fuel and cladding initial temperature (as listed in Table 3-1)
Cladding failure rate	0.1%
Cladding alloy	Zircaloy-4, ZIRLO, and M5
Burnup	40, 50, and 62 GW-day/MTU
Radiolysis kinetics	Exponential decomposition in 4.8 and 72.2 years
Residual water amount*	5.5 and 10 moles
Thermal decay constant	a equal to 0.023 or 0.064
Mode of oxygen contacting the fuel	through grain boundaries
*1 mole of water is not considered in the analysis.	

Table 4-2. Values of Varying Parameters and Corresponding Cases for Presenting the Simulation Data of the Integrated Model

Case No.	Values of Varying Parameters Listed in Table
1	Residual water amounts: 5.5 and 10 moles. Cladding failure rate of 0.1%. Low- and high-end initial fuel temperature. Oxygen diffusion through grain boundaries and contacting each grain simultaneously. Cladding alloy and burnup: Zircaloy-4 and 40, 50, and 62 GW-day/MTU. Thermal decay constant a equal to 0.023. Exponential decomposition of the residual water in 4.8 years.
2	All parameters are the same as Case 1 except decomposition of the residual water in 72.2 years.
3	All parameters are the same as Case 1 except ZIRLO as cladding alloy.
4	All parameters are the same as Case 3 except decomposition of the residual water in 72.2 years.
5	All parameters are the same as Case 1 except M5 as cladding alloy.
6	All parameters are the same as Case 5 except decomposition of the residual water in 72.2 years.
7-12	All parameters are the same as Cases 1-6 except a equal to 0.064, for example, Case 7 parameters are same as Case 1 except a equal to 0.064, and so on.

The simulation data for fuel and cladding oxidation for the twelve cases are presented in various tables. Various parameters are varied independently. The cladding oxidation data are presented in terms of the thickness of the zirconium oxide layer. The fuel oxidation data are presented in terms of the amount of UO_{2+x} phase that would form due to exposure to oxygen produced by radiolysis. The fuel oxidation data also include the extent of oxidation, which is equal to the percentage of the exposed fuel pellets that have undergone oxidation to U_3O_8 phase. The extent of oxidation is separately calculated for the directly exposed fuel pellets and the fuel pellets in the extended crack length that are not directly exposed. The fuel oxidation data are listed in Tables A1-1 to A1–12. The data from these tables are selected to highlight the effects of various varying parameters.

4.1 Cladding Oxidation

Cladding oxidation in general was found to be minimal and was no more than 1-2 micrometer for each cladding alloy with residual water content of 5.5 and 10 moles. Effects of various factors on cladding oxidation are discussed next.

4.1.1 Spent Nuclear Fuel and Cladding Initial Temperatures

The cladding oxidation data from Case 1, i.e., exponential decay to full consumption of residual water in 4.8 years, are extracted to illustrate the effect of fuel and cladding initial temperatures. The cladding oxidation data for 10 moles of residual water, 0.1 percent cladding failure rate, and low- and high-end fuel and cladding initial temperatures are presented in Figure 4–1. Following observations are made. Overall, extent of cladding oxidation is low compared to the initial cladding thickness of 600 μm. More cladding oxidizes with a 400 °C peak temperature compared to a 302 °C peak temperature. For a peak temperature of 400 °C, Zone 2 cladding oxidation, with local high oxygen conditions due to high radiolysis conditions, is more than the Zone 1. This is contrary to the expected trend of increasing cladding oxidation with increasing temperature.

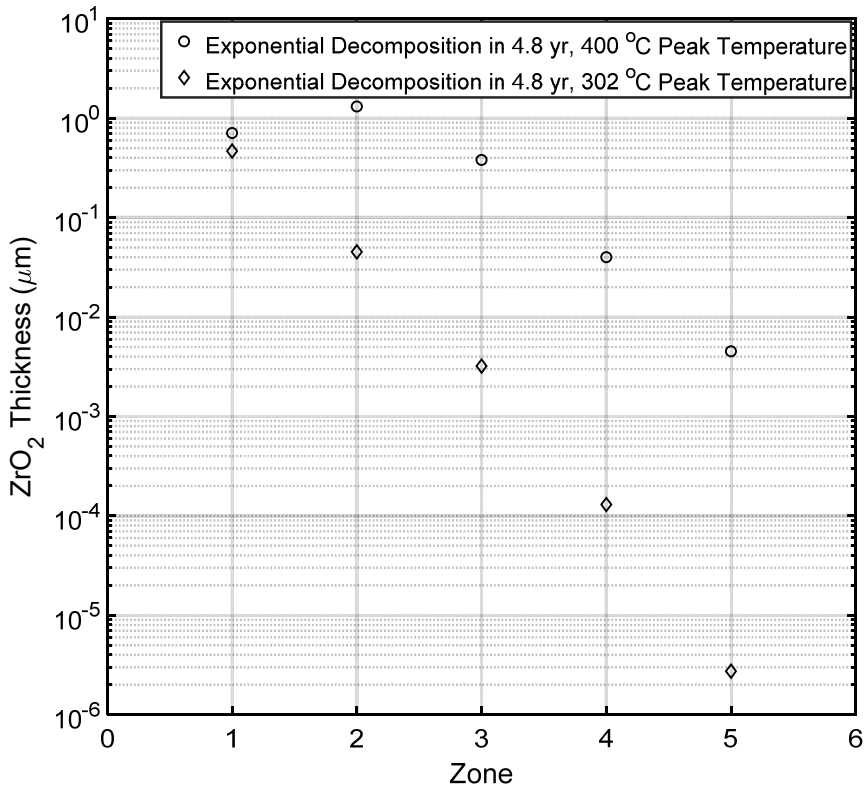

Figure 4–1. ZrO_2 Oxide Layer Thickness Formed During Cladding Oxidation for Case 1 Conditions, Using Two Different Peak Cladding Temperatures and 10 Moles of Residual Water

The reason for the aforementioned observation is following. In the canister, the rates of cladding and fuel oxidation are not only dependent upon temperature but also on the location-specific rate of radiolysis of water and the amount of available oxygen. The amount of available oxygen in a zone is also affected by the transfer of oxygen between the zones in the integration model. In Figure 4–1, cladding oxidation rates for Zones 2 to 5 are lower for the low-end fuel and cladding initial temperature condition compared to the high-end fuel and cladding initial temperature condition because sufficient amount oxygen is available for

the both temperature conditions. Therefore, more oxidation of cladding occurs for Zones 2 to 5 for the high-end, i.e., 400 °C, temperature condition compared to the 302 °C condition. However, at 400 °C in Zone 2, the rate of cladding oxidation is dependent upon the amount of oxygen available in a given time step. More oxygen became available in Zone 2 compared to Zone 1 in the integration model, therefore more oxidation occurred for Zone 2 cladding compared to Zone 1 for the 400 °C condition.

4.1.2 Radiolysis Kinetics

Uncertainty in radiolysis kinetics affects the extent of cladding oxidation by less than one micrometer, which is insignificant compared to the extent of cladding oxidation in the reactor. Cladding oxidation data for Cases 1 and 2 are compared, with peak cladding temperature of 400 °C. The integration model data indicate that radiolysis kinetics affects the cladding oxidation in the case of slower radiolysis kinetics. The cladding oxidation data is shown in Figure 4–2. As seen in the figure, the extent of cladding oxidation is more in Zones 1-3 when residual water decomposes in 4.8 years compared to 72.2 years. However, no difference in the ZrO_2 thickness is noted for Zones 4, and 5. These observations are attributed to the compound effect of the fuel temperature, oxygen generation rate, and amount of available oxygen in a zone. When water decomposes 4.8 years, more oxygen is available within the first 10 years after storage than when water decomposes in 72.2 years. The cladding oxidation in Zones 4 and 5 is dependent upon temperatures, whereas in Zones 1, 2, and 3, the cladding oxidation is dependent upon the rate of oxygen generation and amount of available oxygen. Because more oxygen is generated with the 4.8 years exponential kinetics and more oxygen becomes available, greater oxidation of cladding occurs in Zones 1, 2, and 3 compared to the 72.2 years exponential kinetics.

4.1.3 Water Amount

It is observed that more cladding oxidation occurs for higher amounts of residual water. This trend is observed for all cases and is independent of cladding failure rate. Figure 4–3 shows Cases 1 data to highlight effect of residual water on cladding oxidation. As seen in the figure, Zones 1 and 2 cladding oxide thickness increased with increased amount of residual water. It is observed that in Zones 3-5, cladding oxide thickness is independent of the water amount. This is because Zones 3-5 cladding oxidation rates are temperature dependent, and because of low temperatures in Zones 3-5, cladding oxidation became independent of oxygen available from radiolysis of residual water.

4.1.4 Thermal Decay Constant

Fuel and cladding temperatures are exponentially time-dependent on the thermal decay constant. Fuel and cladding temperature decays faster for a decay constant of 0.064 (Case 7) compared to 0.023 (Case 1). Cladding oxidation data for Cases 1 and 7 are compared, and presented in Figure 4–4. The data are for 10 moles of residual water, 4.8 years exponential decay, 0.1% cladding failure rate, and initial peak cladding temperature of 400 °C. As seen in the figure, Zones 2-4 cladding oxide thickness is more for the 0.023 (Case 1) decay constant compared to 0.064 (Case 7). This is because temperature decreases more rapidly for 0.064 (Case 7) compared to 0.023 (Case 1). As a result, cladding remains at higher temperature for 0.023 (Case 1) decay constant compared to 0.064 (Case 7), and hence more cladding oxidation occurs as cladding oxidation rates are temperature dependent. In Zone 1, the cladding oxidation for 0.064 (Case 7) decay constant is slightly more than 0.023 (Case 1). This is because more net oxygen becomes available in Zone 1 for 0.064 (Case 7) decay constant compared to 0.023 (Case 1) in the integration model; as a result, slightly more cladding oxidation occurs.

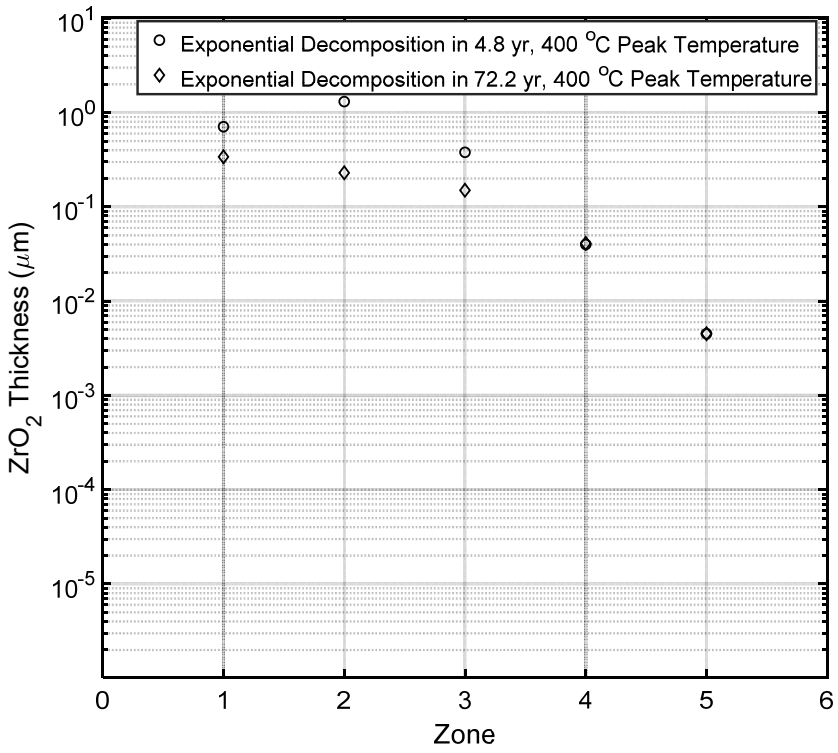

Figure 4–2. ZrO2 Oxide Layer Thickness Formed During Cladding Oxidation in Cases 1 and 2, for 10 Moles of Residual Water

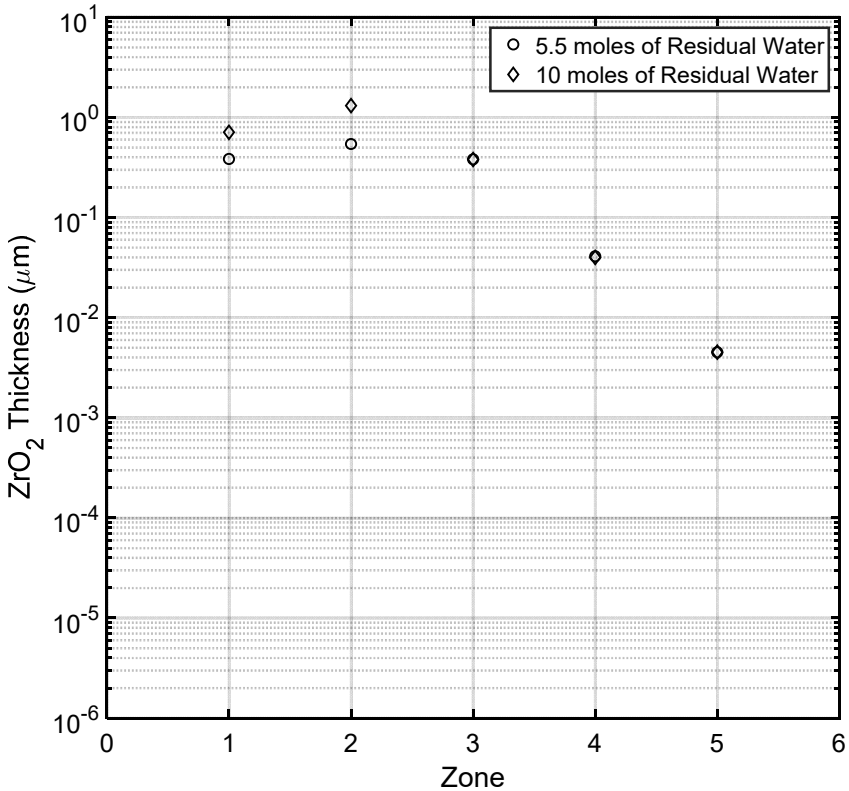

Figure 4–3. ZrO2 Oxide Layer Thickness Formed During Cladding Oxidation in Case 1, for 5 and 10 Moles of Residual Water

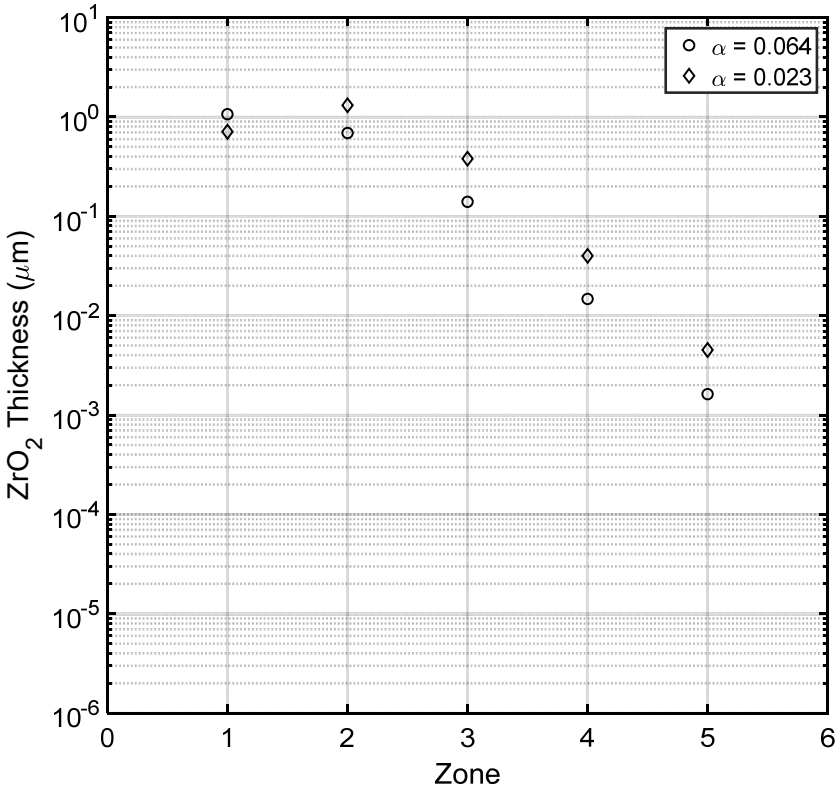

Figure 4–4. ZrO2 Oxide Layer Thickness Formed During Cladding Oxidation in Cases 1 and 7, for 10 Moles of Residual Water

4.1.5 Cladding Type

Effect of cladding type is discussed using Cases 7, 9, and 11 simulation results. The cladding oxidation data is presented in Figure 4–5. As seen in the figure, the oxide thickness data is consistent with the cladding oxidation rates developed in section 3.3; Zircaloy-4 oxide thickness is highest, followed by ZIRLO, and M5 in Zones 2–5. In Zone 1, ZIRLO oxide thickness is slightly more than Zircaloy-4. This is because clad oxidation in the integration model is not only dependent on temperature but also on oxygen availability. For ZIRLO, because less oxygen is consumed in Zones 2-4 compared to Zircaloy-4, more oxygen becomes available in Zone 1. Overall, the cladding oxidation was found to be consistent with the cladding oxidation kinetics model described in Section 3.4.

4.1.6 Burnup

Little to no effect was observed on cladding oxidation extent due to fuel burnup. Fuel oxidation require a small quantity of oxygen. For example, it takes approximately 0.013 moles of oxygen to completely oxidize a fuel pellet from UO_2 to U_3O_8, whereas cladding oxidation consumes most of the oxygen generated by radiolysis. No effect on cladding oxidation was observed when peak cladding temperature was 400 °C. This is because even the high burnup fuel oxidized in accordance with the fuel oxidation model and fuel and cladding temperature distribution with chosen peak temperature of 400 °C. Some effect was observed on cladding oxidation when a lower peak cladding temperature of 302 °C was used, but the effect was negligible.

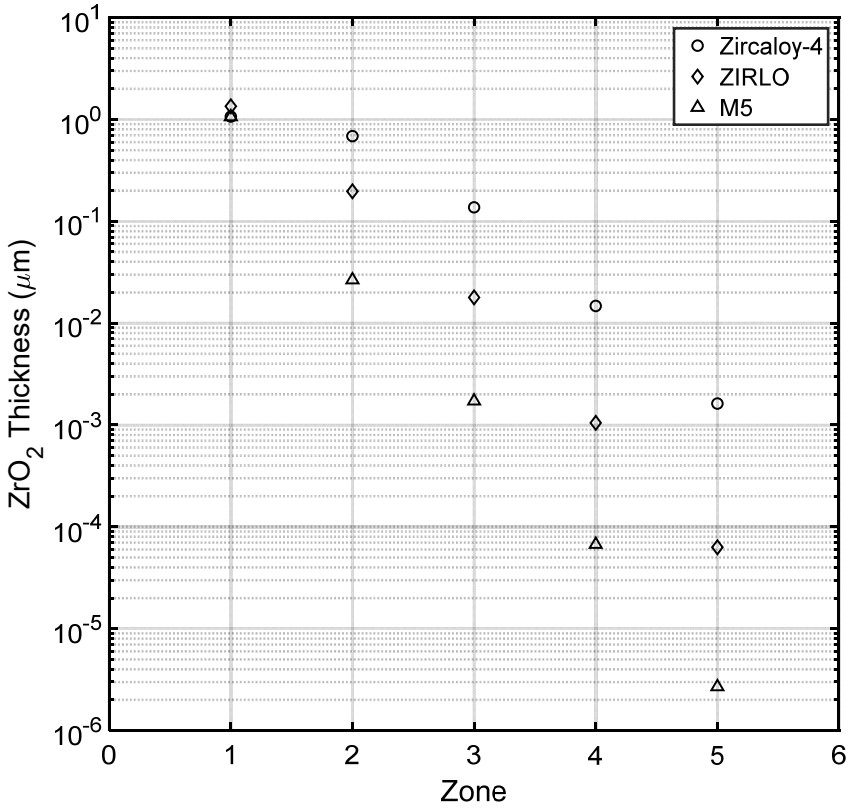

Figure 4–5. ZrO2 Oxide Layer Thickness Formed During Cladding Oxidation for Cases 7, 9, and 11, for 10 Moles of Residual Water

4.2 Spent Nuclear Fuel Oxidation

Depending on the available amount of oxidant (oxygen), the amount of U_3O_8 formed at the defect area will vary. If oxidation rate to form U_3O_8 is slow enough and the oxidant is abundant, the fuel oxidation kinetics will control the rate of U_3O_8 formation. But if the oxidant is limited due to a limited amount of oxygen, the production rate of oxidant from the radiolysis process and subsequent reactions, i.e., reactions between oxidants and cladding plus fuel, will control the overall reaction to form U_3O_8.

4.2.1 Spent Nuclear Fuel and Cladding Initial Temperatures

The fuel oxidation data from Case 1 (exponential in 4.8 years) are extracted to illustrate the temperatures effect. The fuel oxidation data for low- and high-end fuel temperatures conditions, 0.1 percent cladding failure rate, exponential decomposition of the residual water in 4.8 years, 5.5 moles of water, and decay constant equal to 0.023 are listed in Table 4-3.

The listed data indicate that more of the exposed fuel is oxidized at the low-end temperature condition than for the high-end. However, U_3O_8 in temperature Zone 3 for the 302 °C initial cladding temperature is nil for both water amounts, whereas U_3O_8 for the 400 °C condition in Zone 3 is 2.5 and 68.2 g for 5.5 and 10 moles of residual water, respectively. Lower amounts of fuel oxidized in Zones 1 and 2 for 400 °C peak cladding initial temperature compared to the 302 °C cladding temperature because fuel and cladding oxidation simultaneously occur in the integration model, and competition and distribution for oxygen, generated by radiolysis, is determined by oxidation rates and relatives surface areas of fuel and cladding. Because cladding oxidation rate increases with increasing temperature, more cladding oxidizes

at the 400 °C peak temperature condition compared to the 302 °C condition, leaving less oxygen for fuel oxidation in Zones 1 and 2.

To further examine this trend, the fuel oxidation data from the 12 cases for 0.1 percent cladding failure rate and Zircaloy-4, ZIRLO, and M5 cladding types with burnup of 40 GW-day/MTU are listed in Table 4-4. Similarly, the fuel oxidation data from the 12 cases for burnups of 50 and 62 GW-day/MTU are listed in Table 4-5 and Table 4-6, respectively. The mass of U_3O_8 formed due to oxidation in the canister in the five zones is added and listed in Table 4-4 to Table 4-6. Following observations are made regarding the effect of temperature on fuel and cladding oxidation:

- For 5.5 and 10 moles of residual water, more of the exposed fuel is oxidized at the 302 than at 400 °C temperature condition with Zircaloy-4 and fuel burnup of 40 and 50 GW-day/MTU and 0.023 decay constant, and radiolysis in 4.8 years. This is because, at lower fuel and cladding temperature condition, more oxygen becomes available for fuel oxidation with Zircaloy-4 cladding type.

- For ZIRLO and M5, more fuel oxidation occurs with the 400 °C temperature condition compared to the 302 °C condition for all fuel burnups, and with 0.023 decay constant, and radiolysis in 4.8 years. This is because ZIRLO and M5 oxidation rates are much lower than Zircaloy-4, as a result, more oxygen becomes available and fuel oxidizes at higher rate at higher temperature.

- For radiolytic decomposition in 72.2 years, generally more fuel oxidation occurs at 400 °C temperature condition than at 302 °C condition. Only exceptions to this observation is Zircaloy-4, with burnup of 40 GW-day/MTU and decay constants of 0.023 and 0.064.

Table 4-3. Mass of U3O8 Phase and Extent of Oxidation for Exponential Decomposition of the Residual Water in 4.8 Years, 0.1 Percent Cladding Failure Rate, 5.5 and 10 Moles of Water, 0.023 Decay Constant, 40 GW-day/MTU Burnup, and Zircaloy-4 Cladding

Zone	302 °C Peak Cladding Initial Temperature		400 °C Peak Cladding Initial Temperature	
	Mass (g) of U_3O_8 for 5.5 Moles	Mass (g) of U_3O_8 for 10 Moles	Mass (g) of U_3O_8 for 5.5 Moles	Mass (g) of U_3O_8 for 10 Moles
1	68.2	68.2	2.3	4.2
2	66.1	68.2	2.3	6.8
3	0.0	0.0	2.5	68.2
4	0.0	0.0	0.0	0.0

Table 4-4. Mass of U3O8 for Different Water Amount Under Cases 1 to 12. The Data Are for 0.1 Percent Cladding Failure Rate, Fuel Burnup of 40 GW-day/MTU. The Fuel Oxidation Data for the Five Zones Are Added.				
Case Number	**302 °C Peak Cladding Initial Temperature**		**400 °C Peak Cladding Initial Temperature**	
	Combined Mass of U_3O_8 (g) for Water Amount (moles)		**Combined Mass of U_3O_8 for Water Amount (moles)**	
	5.5 moles	**10 moles**	**5.5 moles**	**10 moles**
1 (4.8 years, α = 0.023, Zircaloy-4)	134.3	136.4	4.6	11.0
2 (72.2 years, α = 0.023, Zircaloy-4)	0.5	53.7	1.5	21.3
3 (4.8 years, α = 0.023, ZIRLO)	135.9	136.4	95.4	147.5
4 (72.2 years, α = 0.023, ZIRLO)	23.2	68.2	27.3	140.9
5 (4.8 years, α = 0.023, M5)	136.1	136.5	100.5	191
6 (72.2 years, α = 0.023, M5)	23.3	68.2	54.8	151.1
7 (4.8 years, α = 0.064, Zircaloy-4)	88.9	100.5	204.5	204.5
8 (72.2 years, α = 0.064, Zircaloy-4)	0.2	14.2	0.6	4.5
9 (4.8 years, α = 0.064, ZIRLO)	89.7	101.1	204.6	204.6
10 (72.2 years, α = 0.064, ZIRLO)	0.2	25.9	0.6	54.7
11 (4.8 years, α = 0.064, M5)	89.8	101.1	204.5	204.7
12 (72.2 years, α = 0.064, M5)	0.2	28.2	0.3	63.6

Table 4-5. Mass of U3O8 for Different Water Amount Under Cases 1 to 12. The Data Are for 0.1 Percent Cladding Failure Rate, Fuel Burnup of 50 GW-day/MTU. The Fuel Oxidation Data for the Five Zones Are Added.				
Case Number	**302 °C Peak Cladding Initial Temperature**		**400 °C Peak Cladding Initial Temperature**	
	Combined Mass of U_3O_8 (g) for Water Amount (moles)		**Combined Mass of U_3O_8 for Water Amount (moles)**	
	5.5 moles	**10 moles**	**5.5 moles**	**10 moles**
1 (4.8 years, α = 0.023, Zircaloy-4)	68.2	68.2	4.4	10.2
2 (72.2 years, α = 0.023, Zircaloy-4)	0.1	0.2	0.9	1.7
3 (4.8 years, α = 0.023, ZIRLO)	68.3	68.3	94.5	147.1
4 (72.2 years, α = 0.023, ZIRLO)	0.1	0.4	0.9	24.4
5 (4.8 years, α = 0.023, M5)	68.2	68.3	100.2	190.1
6 (72.2 years, α = 0.023, M5)	0.1	0.4	0.9	45.2
7 (4.8 years, α = 0.064, Zircaloy-4)	68.2	68.2	46.1	204.5
8 (72.2 years, α = 0.064, Zircaloy-4)	0.0	0.1	0.3	0.6
9 (4.8 years, α = 0.064, ZIRLO)	68.2	68.3	159.3	204.6
10 (72.2 years, α = 0.064, ZIRLO)	0.0	0.1	0.4	0.7
11 (4.8 years, α = 0.064, M5)	68.2	68.2	159.4	204.7
12 (72.2 years, α = 0.064, M5)	0.0	0.1	0.4	0.7

Table 4-6. Mass of U3O8 for Different Water Amount Under Cases 1 to 12. The Data Are for 0.1 Percent Cladding Failure Rate, Fuel Burnup of 62 GW-day/MTU. The Fuel Oxidation Data for the Five Zones Are Added.				
Case Number	**302 °C Peak Cladding Initial Temperature**		**400 °C Peak Cladding Initial Temperature**	
	Combined Mass of U_3O_8 (g) for Water Amount (moles)		**Combined Mass of U_3O_8 for Water Amount (moles)**	
	5.5 moles	**10 moles**	**5.5 moles**	**10 moles**
1 (4.8 years, α = 0.023, Zircaloy-4)	0.0	0.0	3.7	8.6
2 (72.2 years, α = 0.023, Zircaloy-4)	0.0	0.0	0.5	0.9
3 (4.8 years, α = 0.023, ZIRLO)	0.0	0.0	4.9	77.6
4 (72.2 years, α = 0.023, ZIRLO)	0.0	0.0	0.5	0.9
5 (4.8 years, α = 0.023, M5)	0.0	0.0	31.9	119.3
6 (72.2 years, α = 0.023, M5)	0.0	0.0	0.5	1.0
7 (4.8 years, α = 0.064, Zircaloy-4)	0.0	0.0	2.4	12.7
8 (72.2 years, α = 0.064, Zircaloy-4)	0.0	0.0	0.2	0.3
9 (4.8 years, α = 0.064, ZIRLO)	0.0	0.0	48.3	136.4
10 (72.2 years, α = 0.064, ZIRLO)	0.0	0.0	0.2	0.3
11 (4.8 years, α = 0.064, M5)	0.0	0.0	136.4	136.6
12 (72.2 years, α = 0.064, M5)	0.0	0.0	0.2	0.3

4.2.2 Radiolysis Kinetics

Data in Tables 4–4, 4–5, and 4–6 are analyzed to delineate the effect of radiolysis kinetics on fuel oxidation. In general, more fuel oxidation occurs when a given amount of water undergoes radiolytic decomposition to completion in 4.8 years compared to completion in 72.2 years, except for the 302 °C temperature condition and 62 GW-day/MTU. No fuel oxidation occurs for combination of 302 °C temperature condition and 62 GW-day/MTU because temperature needed to oxidize UO_2 to U_3O_8 is 327 °C whereas the peak fuel and cladding temperature is 302 °C.

4.2.3 Water Amount

The data compiled in Tables 4–4 to 4–6 also illustrate the effect of water amount on fuel oxidation. The oxidized fuel amounts increase with increasing water because the amount of oxygen produced by radiolysis also increases with increasing water. This trend is observed for all twelve cases, including all cladding types, burnups and radiolysis kinetics. For example, the data in Table 4-4 for Case 1 and the 302 °C temperatures condition, the amount of U_3O_8 is 134.3 g for 5.5 moles of the residual water, whereas the U_3O_8 is 136.4 g for 10 moles of residual water. Sometime, the difference between the oxidized fuel amounts are 10s of grams for a given condition compared to others, however, the trend is always towards more fuel oxidation with increasing residual water amount.

4.2.4 Thermal Decay Constant

An examination of fuel oxidation data for all twelve cases results is summarized in following two observations:

- For fuel burnup of 40 GW-day/MTU and radiolytic decomposition in 4.8 and 72.2 years, fuel oxidation extent is higher for the 0.023 decay constant compared to 0.064 decay constant for the 302 °C temperature condition. For the same set of conditions but burnup of 50 GW-day/MTU, there is no significant difference in the fuel oxidation extent between the two decay constants.

- For fuel burnups of 40, 50, and 62 GW-day/MTU and radiolytic decomposition in 4.8 years, fuel oxidation extent is higher for the 0.064 decay constant compared to the 0.023 constant at the 400 °C temperature condition. For the same set of conditions assuming radiolytic decomposition in 72.2 years, this trend is reversed.

In the integration model, when radiolytic decomposition occurs in 4.8 years, a higher decay constant at the higher peak temperature results in more oxygen available for fuel oxidation. For instance, more fuel oxidizes for the 0.064 decay constant compared to the 0.023 constant at the 400 °C temperature condition.

4.2.5 Cladding Type

Cladding type directly impacts extent of fuel oxidation by affecting oxygen availability. Zircaloy-4 oxidation rates are higher than ZIRLO, followed by M5. It is observed that for a given water amount, radiolysis kinetics, temperature condition, and fuel burnup, more fuel oxidized for M5 cladding compared to ZIRLO, followed by ZIrcaly-4. Few exceptions to this observation are following:

- For burnup of 62 GW-day/MTU and the 302 °C temperature condition, no effect of cladding type is seen because the threshold fuel oxidation temperature is more than the temperature condition.

- For radiolysis is 72.2 years, 0.064 thermal decay, and 5.5 moles of residual water, cladding types do not impact fuel oxidation extent. Same observation is made for radiolysis is 72.2 years, 0.023 thermal decay, 10 moles of residual water and 400 °C temperature condition.

4.2.6 Burnup

More low burn fuel oxidizes for a given set of conditions compared to high burnup fuel. This observation is consistent with the fuel oxidation kinetics model developed for this work. Cladding type directly impact extent of fuel oxidation by affecting oxygen availability. Zircaloy-4 oxidation rates are higher than ZIRLO, followed by M5. It is observed that for a given water amount, radiolysis kinetics, temperature condition, and fuel burnup, more fuel oxidized M5 compared to ZIRLO followed by ZIrcaly-4. Few exceptions to this observation are following:

- For burnup of 62 GW-day/MTU and the 302 °C temperature condition, no effect of cladding type is seen because the threshold fuel oxidation temperature is more than the temperature condition.

- For radiolysis in 72.2 years, 0.064 thermal decay, and 5.5 moles of residual water, cladding types do not impact fuel oxidation extent. Same observation is made for radiolysis in 72.2 years, 0.023 thermal decay, 10 moles of residual water and 400 °C temperature condition.

4.3 Cladding Failure

Fuel oxidation data and 80 percent conversion criterion corresponding to approximately 6.5 percent strain in Table 3-6 are used to determine risk of cladding gross rupture. Various cases listed in Table 4-2 are analyzed for their fuel oxidation extent and compared to the 80 percent conversion criterion, i.e., 80 Percent of UO_2 in a Fuel Pellet Converts to U_3O_8. Fuel oxidation data listed in Tables A1-1 to A1-12 was compared to the criterion using the following approach. In the integration model, two fuel pellets are located underneath the 3.5 cm long crack and four pellets under the extended length, i.e., crack length plus 3 cm on both side of the crack. The two pellets directly underneath the crack undergo fuel oxidation first, followed by the four fuel pellets under crack length plus 3 cm on both sides provided enough leftover oxygen is available. Oxidation of one fuel pellet results in approximately 11.35 g of U_3O_8 in the integration model. The cladding failure risk is considered to be present when any fuel pellet has undergone 80 percent conversion to U_3O_8. The risk data is presented in following three categories: (a) "No" risk of cladding failure — fuel oxidation extent was less than 80 percent, (b) "Yes" risk of cladding failure — fuel oxidation extent was more than 80 percent for the fuel pellets directly underneath the crack length and fuel pellets in the 6 cm zone beyond the crack, and (c) "Yes*" risk of cladding failure — fuel oxidation extent at least more than 80 percent for the fuel pellets directly underneath the crack, but not necessarily for the fuel pellets in the 6 cm zone beyond the crack. The analysis of fuel oxidation data meeting the criterion is presented in Table 4-7. The data in the table are organized in the order of radiolysis time, thermal decay constant, and cladding type. Following observations are made using the data listed in Table 4-7:

- For the peak cladding temperature condition of 302 °C and radiolytic decomposition in 4.8 years, the risk of cladding failure is same for 5.5 and 10 moles of residual water. The cladding failure risk is independent of the thermal decay constant for these set of conditions.

- For the peak cladding temperature condition of 400 °C and radiolytic decomposition in 4.8 years, the risk of cladding failure is become higher with lesser oxidizing cladding alloy for a given amount of residual water and burnup. The cladding failure risk also increases with higher value of the thermal decay constant for a given set of conditions.

Table 4-7. Cladding Failure Risk Due to Fuel Oxidation as per the 80 Percent Conversion Criterion, i.e., 80 Percent of UO_2 in a Fuel Pellet Converts to U_3O_8

Case	Burnup (GW-day/MTU	302 °C Peak Cladding Initial Temperature		400 °C Peak Cladding Initial Temperature	
		5.5 Moles	10 Moles	5.5 Moles	10 Moles
1 (4.8 years, α = 0.023, Zircaloy-4)	40	**Yes**	**Yes**	**Yes**	**Yes**
	50	**Yes**	**Yes**	No	**Yes**
	62	No	No	No	No
3 (4.8 years, α = 0.023, ZIRLO)	40	**Yes**	**Yes**	**Yes**	**Yes**
	50	**Yes**	**Yes**	**Yes**	**Yes**
	62	No	No	No	**Yes**
5 (4.8 years, α = 0.023, M5)	40	**Yes**	**Yes**	**Yes**	**Yes**
	50	**Yes**	**Yes**	**Yes**	**Yes**
	62	No	No	**Yes***	**Yes**
7 (4.8 years, α = 0.064, Zircaloy-4)	40	**Yes**	**Yes**	**Yes**	**Yes**
	50	**Yes**	**Yes**	**Yes***	**Yes**
	62	No	No	No	No
9 (4.8 years, α = 0.064, ZIRLO)	40	**Yes**	**Yes**	**Yes**	**Yes**
	50	**Yes**	**Yes**	**Yes**	**Yes**
	62	No	No	**Yes***	**Yes**
11 (4.8 years, α = 0.064, M5)	40	**Yes**	**Yes**	**Yes**	**Yes**
	50	**Yes**	**Yes**	**Yes**	**Yes**
	62	No	No	**Yes**	**Yes**
2 (72.2 years, α = 0.023, Zircaloy-4)	40	No	**Yes***	No	**Yes***
	50	No	No	No	No
	62	No	No	No	No
4 (72.2 years, α = 0.023, ZIRLO)	40	**Yes***	**Yes**	**Yes***	**Yes**
	50	No	No	No	**Yes***
	62	No	No	No	No
6 (72.2 years, α = 0.023, M5)	40	**Yes***	**Yes**	**Yes***	**Yes**
	50	No	No	No	**Yes***
	62	No	No	No	No
8 (72.2 years, α = 0.064, Zircaloy-4)	40	No	No	No	No
	50	No	No	No	No
	62	No	No	No	No
10 (72.2 years, α = 0.064, ZIRLO)	40	No	**Yes***	No	**Yes***
	50	No	No	No	No
	62	No	No	No	No
12 (72.2 years, α = 0.064, M5)	40	No	**Yes***	No	**Yes***
	50	No	No	No	No
	62	No	No	No	No

Yes*: fuel pellets directly underneath the crack underwent at least 80 percent conversion, but not necessarily the pellets in the 6 cm zone beyond the crack

- For the peak cladding temperature condition of 302 °C, radiolytic decomposition in 72.2 years, and thermal decay constant equal to 0.023, there is no risk of cladding failure when fuel burnups are 50 and 62 GW-day/MTU. The risk of cladding failure is categorized as Yes* when fuel burnup is 40 GW-day/MTU, Zircaly-4 cladding, and 10 moles of residual water. The cladding

  failure risk increases with lesser oxidizing cladding alloy and lower water amount for 40 GW-day/MTU burnup under these set of conditions, but the increase is only marginal.

- For the peak cladding temperature condition of 400 °C, radiolytic decomposition in 72.2 years, and thermal decay constant equal to 0.023, the risk of cladding failure occurs for 40 GW-day/MTU burnup and 10 moles of residual water with all three cladding materials. The risk also exists for 50 GW-day/MTU burnup for ZIRLO and M5 claddings and 10 moles of residual water.

- For the peak cladding temperature conditions of 302 and 400 °C, radiolytic decomposition in 72.2 years, and thermal decay constant equal to 0.023 and 0.064, the risk of cladding failure exist only when residual water is 10 moles, fuel burnup is 40 GW-day/MTU, and cladding types are ZIRLO and M5.

Overall, it is observed that the risk of cladding failure is more likely under higher radiation field, i.e., when radiolytic decomposition of the residual water occurs in few years compared to several decades. The fuel oxidation simulation data also indicate that the failure risk is more for the higher values of fuel and cladding temperatures compared to the lower values.

5. SUMMARY, CONCLUSIONS, and FUTURE REFINEMENTS

Results of the gas sampling analysis under the high burnup cask demonstration project have shown residual water amount to be approximately 100 mL, i.e., 5.5 moles (Bryan et al., 2019). Considering uncertainty is determining the residual water amount, an analysis was conducted using 5.5 and 10 moles of residual water. The analysis was conducted to determine extent of fuel and cladding oxidation due to radiolysis of residual water. An integrated modeling approach was used, interlinking evolution of fuel and cladding temperatures, radiolysis of residual water, cladding oxidation and its dependence of temperature and cladding alloy, and fuel oxidation and its dependence on temperature, relative humidity and burnup. The integrated model's results provide following insight:

- Extent of cladding oxidation is no more than 2 μm additional consumption of the cladding metal even with 10 moles of residual water, indicating that changes in cladding conditions due to residual water are expected to be negligible,

- Fuel oxidation, significant to extend the breach opening size, could occur even with 5.5 moles of residual water, especially when radiolytic decomposition of the residual water occurs in a few years compared to a few decades, and

- Risk of cladding failure directly correlate with extent of fuel oxidation. The fuel oxidation results indicate that risk of cladding failure is more likely under higher radiation field, i.e., when radiolytic decomposition of the residual water occurs in few years compared to several decades. The fuel oxidation simulation data also indicate that the failure risk is more for the higher fuel and cladding temperatures compared to the lower temperatures.

One of the key assumptions in the current work is that the radiolytically generated oxygen is equally available to both fuel and cladding, without accounting for the fact that the size of cladding defect is expected to provide some resistance to the transportation of oxygen from the canister cavity to the fuel.

The analyses and results in this work involved synthesis of many separate constitutive materials models with inputs and assumptions to arrive at results for estimation for conditions for cladding failure (initial breach extension). This convolution of information for failure estimation therefore must be regarded having a moderate to high uncertainty for actual failure occurrence with residual water.

Several refinements to this present work are suggested:

- Evaluate the effect of initial defect size (crack size) on transport of radiolytically generated oxygen to further oxidize the fuel within the cladding.

- Update the fuel oxidation model, and its implementation in the integration model.

- Develop the fracture mechanics formulation for cladding failure with updated mechanical properties.

- Estimate the amount of fines released from an extended breach cladding and the physical and radiological characteristics of the fines.

6. REFERENCES

Ahn, T. NUREG–1565, "Dry Oxidation and Fracture of LWR Spent Fuels." ML040150720. Washington, DC: U.S. Nuclear Regulatory Commission. 1996.

ASTM International. "Standard Guide for Drying Behavior of Spent Nuclear Fuel." ASTM C1553–16. West Conshohocken, Pennsylvania: ASTM International. 2016.

Bailey, J.C. and M. Tokar. NUREG/CR–3001, "Fuel Performance Annual Report for 1981." PNL–4342. Washington, DC: U.S. Nuclear Regulatory Commission. December 1982.

Bruno, J. and R.C. Ewing. "Spent Nuclear Fuel." *Elements*. Vol. 2. pp. 343–349. 2006.

Bryan, C.R., S.G. Durbin, E. Lindgren, A.G. Ilgen, T.J. Montoya, T. Dewers, D. Fascitelli. "SNL Contribution: Consequence Analysis for Moisture Remaining in Dry Storage Canisters After Drying," Sandia National Laboratory, SAND2019-8532 R, 2019.

Cheng, B.C., D. Smith, E. Armstrong, K. Tunage, and G. Bond. "Water Chemistry and Fuel Performance in LWRs." Proceedings of the 2000 International Topical Meeting on Light Water Reactor Fuel Performance, Park City, Utah, April 10–13, 2000. Published on CD-ROM. La Grange Park, Illinois: American Nuclear Society. 2000.

Chu, S., Flaw Growth and Flaw Tolerance Assessment for Dry Cask Storage Canisters, No. 3002002785, Electric Power Research Institute, Palo Alto, CA., USA, 2014.

CNWRA. Extended Storage and Transportation: Evaluation of Drying Adequacy. Authors: H. Jung, P. Shukla, T. Ahn, L. Tipton, K. Das, X. He, and D. Basu, San Antonio, Texas: Center for Nuclear Waste Regulatory Analyses. 2013.

EPRI. "Oxidation of Spent Fuel Between 250 and 360 °C." EPRI NP–4524. Palo Alto, California: Electric Power Research Institute. 1986.

EPRI. "Spent Fuel Transportation Applications—Assessment of Cladding Performance A Synthesis Report-Final Report." EPRI-TR-1015048. Palo Alto, California: Electric Power Research Institute. 2007.

Einziger, R.E. and J.A. Cook. "Behavior of Breached Light Water Reactor Spent Fuel Rods in Air and Inert Atmospheres at 229 °C." *Nuclear Technology*. Vol. 69. pp. 55–71. 1985.

Einziger, R.E. and R.V. Strain. "Behavior of Breached Pressurized Water Reactor Spent-Fuel Rods in an Air Atmosphere Between 250 and 360 °C." *Nuclear Technology*. Vol. 75. pp. 82–95. 1986.

Einziger, R.E., L.E. Thomas, H.C. Buchanan, and R.B. Stout. "Oxidation of Spent Fuel in Air At 175 to 195 °C." *Journal of Nuclear Materials*. Vol. 190. pp. 53–60. 1992.

Ghali, E. Corrosion Resistance of Aluminum and Magnesium Alloys: Understanding, Performance and Testing. Hoboken, New Jersey: John Wiley & Sons, Inc. 2010.

Garde, A.M. "Enhancement of Aqueous Corrosion of Zircaloy-4 Due to Hydride Precipitation at the Metal-Oxide Interface." Proceedings of the Zirconium in the Nuclear Industry: 9th International

Symposium. C.M. Eucken and A.M. Garde, eds. ASTM STP 1132. West Conshohocken, Pennsylvania: ASTM International. pp. 566–594. 1991.

Hanson, B.D. "The Burnup Dependence of Light Water Reactor Spent Fuel Oxidation." PNL–11929. Richland, Washington: Pacific Northwest National Laboratory. 1998.

Hastings, I.J., E. Missan, A.M. Ross, J.R. Kelm, R.J. Chenier, D.H. Rose, and J. Novak. "Postirradiation Behavior of UO_2 Fuel: Fragments at 175 to 275 °C in Air." *Nuclear Technology*. Vol. 68. pp. 40–47. 1985.

Herranz, L.E. and F. Feria. "Spent Fuel Rod Splitting Due to UO_2 Oxidation During Dry Storage: Assessment of the Database." *Progress in Nuclear Energy*. Vol. 51. pp. 201–206. 2009.

Jensen, B.J. and D.J. Richmond. "Thermal Analysis of High Decay Heat Loading Strategies in the MAGNASTOR System," Pacific Northwest National Laboratory, PNNL-XXXX, 2019.

Kang, K.H., S.H. Na, K.C. Song, S.H. Lee, S.W. Kim, "Oxidation behavior of the simulated fuel with dissolved fission products in air at 573–873 K," Thermochimica Acta, Vol. 455, pp. 129–133, 2007.

Kansa, E.J., B.D. Hanson, R.B. Stout, "Grain Size and Burnup Dependence of Spent Fuel Oxidation: Geological Repository Impact," In Proceedings of Materials Research Society, Vol. 556, pp. 455-462, 1999.

Kesterson, R., R. Sindelar, and D. Vinson "Used Nuclear Fuel Characteristics at End of Life," Savannah River National Laboratory, SRNL-STI-2013-00181, 2013.

Kim, K.S., G.S. You, D.K. Min, S.G. Ro, E.K. Kim, "Oxidation Behavior of Unirradiated and Irradiated UO_2 in Air at 150-375 °C," Journal of Korean Nuclear Society, Vol. 29, No. 2, pp. 93-98, 1997.

Knight, T. Experimental Determination and Modeling of Used Fuel Drying by Vacuum and Gas Circulation for Dry Cask Storage. Project No. 14-7730. University of South Carolina, 2018.

Laham, S.A., Stress Intensity Factor and Limit Load Handbook, SINTAP Report, Sub-Task 2.6, Nuclear Electric Report EPD/GEN/REP/0316/98, British Energy Generation Ltd, UK, pp. 1998.

Mardon, J. P., G.L. Garner, and P.B. Hoffmann. "M5® A Breakthrough in Zr Alloy." Proceedings of 2010 LWR Fuel Performance/TopFuel/WRFPM, Orlando, Florida, September 26–29, 2010. American Nuclear Society. 2010.

McEachern, R.J. and P. Taylor. "A Review of the Oxidation of Uranium Dioxide at Temperatures Below 400 °C." *Journal of Nuclear Materials*. Vol. 254. pp. 87–121. 1998.

McKinnon, M.A., R.E. Dodge, R.C. Schmitt, L.E. Eslinger, and G. Dineen. "Performance Testing and Analyses of the VSC-17 Ventilated Concrete Cask." TR–100305. Palo Alto, California: Electric Power Research Institute. 1992.

Manzel, R. and C.T. Walker. "EPMA and SEM of Fuel Samples from PWR Rods with an Average Burnup of Around 100 MWd/kgHM." *Journal of Nuclear Materials*. Vol. 301. pp. 170–182. 2002.

Novak, J., I.J. Hastings, E. Mizzan, and R.J. Chenier. "Postirradiation Behavior of UO_2 Fuel: Elements at 220 to 250 °C in Air." *Nuclear Technology*. Vol. 63. pp. 254–265. 1983.

NRC, "Scientific Notebook # 1098E: Development of an Integration Model to Evaluate Effect of Residual Water on Fuel and Cladding Oxidation," ML13144A148, Washington, DC: U.S. Nuclear Regulatory Commission. 2013.

NRC. "Interim Staff Guidance–11, Cladding Considerations for the Transportation and Storage of Spent Fuel, Revision 3." Washington, DC: U.S. Nuclear Regulatory Commission. 2003.

NRC. Interim Staff Guidance–1, "Classifying the Condition of Spent Nuclear Fuel for Interim Storage and Transportation Based on Function." Rev. 2. Washington, DC: U.S. Nuclear Regulatory Commission. 2007.

NRC. NUREG–1536, "Standard Review Plan for Dry Cask Storage Systems." Rev. 1. Washington, DC: U.S. Nuclear Regulatory Commission. July 2010.

NUREG/CR-6846, "Air Oxidation Kinetics for Zr-Based Alloys," U.S. Nuclear Regulatory Commission," ML16112A084, Argonne National Laboratory, 2004.

Radulescu, G. and K. Banerjee, "Detailed Radiation Dose Rate Evaluation of Commercial Spent Nuclear Fuel Canisters," Conference Proceedings of 2015 International High-Level Radioactive Waste Management Conference. American Nuclear Society, Knoxville, Tennessee, 2019.

Raynaud, P.A., D. A. Koss, A. T. Motta, and K. S. Chan, "Fracture Toughness of Hydrided Zircaloy-4 Sheet Under Through-Thickness Crack Growth Conditions," Journal of ASTM International, Vol. 5, No. 1, Paper ID JAI101183, pp. 1-15, 2007.

Rondinella, V. and T. Wiss. "The High Burnup Structure in Nuclear Fuel." *Materials Today*. Vol. 13, No. 12. pp. 24–32. 2010.

Suzuki, M. and S. Kawasaki, "Oxidation of Zircaloy Cladding in Air," Journal of Nuclear Materials. Vol. 140. pp. 32–43. 1986.

Sabol, G.P., R.J. Comstock, R.A. Weiner, P. Larouere, and R.N. Stanutz. "In-Reactor Corrosion Performance of ZIRLO and Zircaloy-4." Proceedings of the Zirconium in the Nuclear Industry: 10th International Symposium. ASTM–STP–1425. A.M. Garde and E.R. Bradley, eds. West Conshohocken, Pennsylvania: American Society for Testing and Materials. pp. 724–744. 1994.

Sindelar, R.L., A. J. Duncan, M. E. Dupont, P. S. Lam, M. R. Louthan, Jr., and T. E. Skidmore, "Materials Aging Issues and Aging Management for Extended Storage and Transportation of Spent Nuclear Fuel," NUREG/CR-7116 (SRNL-STI-2011-00005), Prepared for the Division of Storage and Transportation, Office of Nuclear Reactor Regulation, U.S. Nuclear Regulatory Commission, Washington, DC, November 2011.

Stout, R. and H. Leider, "Preliminary Waste Form Characteristics Report." Version 1.0, UCRL-ID-108314, Lawrence Livermore National Laboratory, Livermore, CA, 1994.

Tada, H., P. C. Paris and G. R. Irwin, "The Stress Analysis of Cracks Handbook," Second Edition, Paris Productions Incorporated (and Del. Research Corporation), Saint Louis, Missouri, 1985.

Taylor, P., D.D. Wood, and D.G. Owen. "Microstructures of Corrosion Films on UO_2 Fuel Oxidized in Air-Steam Mixtures at 225 °C." *Journal of Nuclear Materials*. Vol. 223. pp. 316–320. 1995.

Thomas, L. E., R. E. Einziger, and R E. Woodley, "Microstructural Examination of Oxidized Spent Fuel by Trnasmission Electron Spectroscopy," Journal of Nuclear Materials, Vol. 166, pp. 243-251, 1989.

Thomas, L. E., R. E. Einziger, and H. C. Buchanan, "Effect of Fission Products on Air Oxidation of LWR Spent Fuel," Journal of Nuclear Materials, Vol. 201, pp. 310-319, 1993.

Van Swam, L.F., G.M. Bain, W.C. Dey, D.D. Davis, and H. Heckermann. "BWR and PWR Fuel Performance at High Burnup." Proceedings of the 1997 International Topical Meeting on LWR Performance, Portland, Oregon, March 2–6, 1997. La Grange Park, Illinois: American Nuclear Society. pp. 3–10. 1997.

Wittman, R.S. and B.D. Hanson, "Radiolysis Model Analysis for a Used Fuel Storage Canister," Conference Proceedings of 2015 International High-Level Radioactive Waste Management Conference. American Nuclear Society Charleston, South Carolina, 2015.

Wang, J.A., "Fracture Toughness Evaluation for Spent Nuclear Fuel Clad Systems Using Spiral Notch Torsion Fracture Toughness Test," ORNL/TM-2019/1204, Oak Ridge National Laboratory, Oak Ridge, Tennessee, USA, June 2019.

Wasywich, K.M., W.H. Hocking, D.W. Shoesmith, and P. Taylor. "Differences in Oxidation Behavior of Used CANDU Fuel During Prolonged Storage in Moisture-Saturated Air and Dry Air at 150 °C." *Nuclear Technology*. Vol. 104. pp. 309–329. 1993.

Appendix A: Fuel Oxidation Data

This page intentionally left blank.

Table A1-1. Fuel Oxidation Simulation Data for Case 1 (Exponential Decomposition of the Residual Water in 4.8 Years, Thermal Decay Constant Equal to 0.023, Zircaloy-4 Cladding)

Zone	Low-End Fuel and Cladding Initial Temperatures						High-End Fuel and Cladding Initial Temperatures						Cladding Failure Rate
	Fuel burnup (GW-day/MTU) and residual water amount (moles)												
	40 GW–day/MTU		50 GW–day/MTU		62 GW–day/MTU		40 GW–day/MTU		50 GW–day/MTU		62 GW–day/MTU		
	5.5	10	5.5	10	5.5	10	5.5	10	5.5	10	5.5	10	
	U_3O_8 Mass (g)	U_3O_8 Mass (g)	U_3O_8 Mass (g)	U_3O_8 Mass (g)	U_3O_8 Mass (g)	U_3O_8 Mass (g)	U_3O_8 Mass (g)	UO_{2+x} Mass (g)	U_3O_8 Mass (g)	U_3O_8 Mass (g)	U_3O_8 Mass (g)	U_3O_8 Mass (g)	
1	68.2	68.2	68.2	68.3	0.0	0.0	2.3	4.2	2.3	4.2	2.1	3.9	0.1
2	66.1	68.2	0.0	0.0	0.0	0.0	2.3	6.8	2.1	6.1	1.6	4.7	0.1
3	0.0	0.0	0.0	0.0	0.0	0.0	2.5	68.2	1.3	68.2	0.0	0.0	0.1
4	0.0	0.0	0.0	0.0	0.0	0.0	0.0	0.0	0.0	0.0	0.0	0.0	0.1

Table A1-2. Fuel Oxidation Simulation Data for Case 2 (Exponential Decomposition of the Residual Water in 72.2 Years, Thermal Decay Constant Equal to 0.023, Zircaloy-4 Cladding)

Zone	Low-End Fuel and Cladding Initial Temperatures						High-End Fuel and Cladding Initial Temperatures						Cladding Failure Rate
	Fuel burnup (GW-day/MTU) and residual water amount (moles)												
	40 GW–day/MTU		50 GW–day/MTU		62 GW–day/MTU		40 GW–day/MTU		50 GW–day/MTU		62 GW–day/MTU		
	5.5	10	5.5	10	5.5	10	5.5	10	5.5	10	5.5	10	
	U_3O_8 Mass (g)	U_3O_8 Mass (g)	U_3O_8 Mass (g)	U_3O_8 Mass (g)	U_3O_8 Mass (g)	U_3O_8 Mass (g)	U_3O_8 Mass (g)	UO_{2+x} Mass (g)	U_3O_8 Mass (g)	U_3O_8 Mass (g)	U_3O_8 Mass (g)	U_3O_8 Mass (g)	
1	0.5	53.6	0.1	0.2	0.0	0.0	0.7	19.8	0.5	0.9	0.3	0.6	0.1
2	0.0	0.0	0.0	0.0	0.0	0.0	0.5	1.0	0.3	0.6	0.2	0.3	0.1
3	0.0	0.0	0.0	0.0	0.0	0.0	0.3	0.5	0.1	0.2	0.0	0.0	0.1
4	0.0	0.0	0.0	0.0	0.0	0.0	0.0	0.0	0.0	0.0	0.0	0.0	0.1

Table A1-3. Fuel Oxidation Simulation Data for Case 3 (Exponential Decomposition of the Residual Water in 4.8 Years, Thermal Decay Constant Equal to 0.023, ZIRLO Cladding)

Zone	Low-End Fuel and Cladding Initial Temperatures						High-End Fuel and Cladding Initial Temperatures						Cladding Failure Rate
	Fuel burnup (GW-day/MTU) and residual water amount (moles)												
	40 GW–day/MTU		50 GW–day/MTU		62 GW–day/MTU		40 GW–day/MTU		50 GW–day/MTU		62 GW–day/MTU		
	5.5 Moles	10 Moles	5.5 Moles	10 Moles	5.5 Moles	10 Moles	5.5 Moles	10 Moles	5.5 Moles	10 Moles	5.5 Moles	10 Moles	
	U_3O_8 Mass (g)	U_3O_8 Mass (g)	U_3O_8 Mass (g)	U_3O_8 Mass (g)	U_3O_8 Mass (g)	U_3O_8 Mass (g)	U_3O_8 Mass (g)	UO_{2+x} Mass (g)	U_3O_8 Mass (g)	U_3O_8 Mass (g)	U_3O_8 Mass (g)	U_3O_8 Mass (g)	
1	68.2	68.2	68.3	68.3	0.0	0.0	2.3	11.1	2.3	10.7	2.2	9.4	0.1
2	67.7	68.2	0.0	0.0	0.0	0.0	24.9	68.2	24.0	68.2	2.8	68.2	0.1
3	0.0	0.0	0.0	0.0	0.0	0.0	68.2	68.2	68.2	68.2	0.0	0.0	0.1
4	0.0	0.0	0.0	0.0	0.0	0.0	0.0	0.0	0.0	0.0	0.0	0.0	0.1

Table A1-4. Fuel Oxidation Simulation Data for Case 4 (Exponential Decomposition of the Residual Water in 72.2 Years, Thermal Decay Constant Equal to 0.023, ZIRLO Cladding)

Zone	Low-End Fuel and Cladding Initial Temperatures						High-End Fuel and Cladding Initial Temperatures						Cladding Failure Rate
	Fuel burnup (GW-day/MTU) and residual water amount (moles)												
	40 GW–day/MTU		50 GW–day/MTU		62 GW–day/MTU		40 GW–day/MTU		50 GW–day/MTU		62 GW–day/MTU		
	5.5 Moles	10 Moles	5.5 Moles	10 Moles	5.5 Moles	10 Moles	5.5 Moles	10 Moles	5.5 Moles	10 Moles	5.5 Moles	10 Moles	
	U_3O_8 Mass (g)	U_3O_8 Mass (g)	U_3O_8 Mass (g)	U_3O_8 Mass (g)	U_3O_8 Mass (g)	U_3O_8 Mass (g)	U_3O_8 Mass (g)	UO_{2+x} Mass (g)	U_3O_8 Mass (g)	U_3O_8 Mass (g)	U_3O_8 Mass (g)	U_3O_8 Mass (g)	
1	23.2	68.2	0.1	0.4	0.0	0.0	26.5	68.2	0.5	23.5	0.3	0.6	0.1
2	0.0	0.0	0.0	0.0	0.0	0.0	0.5	68.2	0.3	0.6	0.2	0.3	0.1
3	0.0	0.0	0.0	0.0	0.0	0.0	0.3	4.6	0.1	0.2	0.0	0.0	0.1
4	0.0	0.0	0.0	0.0	0.0	0.0	0.0	0.0	0.0	0.0	0.0	0.0	0.1

Table A1-5. Fuel Oxidation Simulation Data for Case 5 (Exponential Decomposition of the Residual Water in 4.8 Years, Thermal Decay Constant Equal to 0.023, M5 Cladding)

Zone	Low-End Fuel and Cladding Initial Temperatures						High-End Fuel and Cladding Initial Temperatures						Cladding Failure Rate
	Fuel burnup (GW-day/MTU) and residual water amount (moles)												
	40 GW–day/MTU		50 GW–day/MTU		62 GW–day/MTU		40 GW–day/MTU		50 GW–day/MTU		62 GW–day/MTU		
	5.5 Moles	10 Moles	5.5 Moles	10 Moles	5.5 Moles	10 Moles	5.5 Moles	10 Moles	5.5 Moles	10 Moles	5.5 Moles	10 Moles	
	U_3O_8 Mass (g)	U_3O_8 Mass (g)	U_3O_8 Mass (g)	U_3O_8 Mass (g)	U_3O_8 Mass (g)	U_3O_8 Mass (g)	U_3O_8 Mass (g)	UO_{2+x} Mass (g)	U_3O_8 Mass (g)	U_3O_8 Mass (g)	U_3O_8 Mass (g)	U_3O_8 Mass (g)	
1	68.2	68.3	68.2	68.3	0.0	0.0	2.4	54.6	3.0	53.7	4.5	51.0	0.1
2	67.9	68.2	0.0	0.0	0.0	0.0	29.9	68.2	29.0	68.2	27.5	68.3	0.1
3	0.0	0.0	0.0	0.0	0.0	0.0	68.2	68.2	68.2	68.2	0.0	0.0	0.1
4	0.0	0.0	0.0	0.0	0.0	0.0	0.0	0.0	0.0	0.0	0.0	0.0	0.1

Table A1-6. Fuel Oxidation Simulation Data for Case 6 (Exponential Decomposition of the Residual Water in 72.2 Years, Thermal Decay Constant Equal to 0.023, M5 Cladding)

Zone	Low-End Fuel and Cladding Initial Temperatures						High-End Fuel and Cladding Initial Temperatures						Cladding Failure Rate
	Fuel burnup (GW-day/MTU) and residual water amount (moles)												
	40 GW–day/MTU		50 GW–day/MTU		62 GW–day/MTU		40 GW–day/MTU		50 GW–day/MTU		62 GW–day/MTU		
	5.5 Moles	10 Moles	5.5 Moles	10 Moles	5.5 Moles	10 Moles	5.5 Moles	10 Moles	5.5 Moles	10 Moles	5.5 Moles	10 Moles	
	U_3O_8 Mass (g)	U_3O_8 Mass (g)	U_3O_8 Mass (g)	U_3O_8 Mass (g)	U_3O_8 Mass (g)	U_3O_8 Mass (g)	U_3O_8 Mass (g)	UO_{2+x} Mass (g)	U_3O_8 Mass (g)	U_3O_8 Mass (g)	U_3O_8 Mass (g)	U_3O_8 Mass (g)	
1	23.3	68.2	0.1	0.4	0.0	0.0	49.0	68.2	0.5	44.5	0.3	0.7	0.1
2	0.0	0.0	0.0	0.0	0.0	0.0	5.5	68.2	0.3	0.6	0.2	0.3	0.1
3	0.0	0.0	0.0	0.0	0.0	0.0	0.3	14.8	0.1	0.2	0.0	0.0	0.1
4	0.0	0.0	0.0	0.0	0.0	0.0	0.0	0.0	0.0	0.0	0.0	0.0	0.1

Table A1-7. Fuel Oxidation Simulation Data for Case 7 (Exponential Decomposition of the Residual Water in 4.8 Years, Thermal Decay Constant Equal to 0.064, Zircaloy-4 Cladding)

Zone	Low-End Fuel and Cladding Initial Temperatures						High-End Fuel and Cladding Initial Temperatures						Cladding Failure Rate
	Fuel burnup (GW-day/MTU) and residual water amount (moles)												
	40 GW–day/MTU		50 GW–day/MTU		62 GW–day/MTU		40 GW–day/MTU		50 GW–day/MTU		62 GW–day/MTU		
	5.5 Moles	10 Moles	5.5 Moles	10 Moles	5.5 Moles	10 Moles	5.5 Moles	10 Moles	5.5 Moles	10 Moles	5.5 Moles	10 Moles	
	U_3O_8 Mass (g)	U_3O_8 Mass (g)	U_3O_8 Mass (g)	U_3O_8 Mass (g)	U_3O_8 Mass (g)	U_3O_8 Mass (g)	U_3O_8 Mass (g)	UO_{2+x} Mass (g)	U_3O_8 Mass (g)	U_3O_8 Mass (g)	U_3O_8 Mass (g)	U_3O_8 Mass (g)	
1	68.2	68.2	68.2	68.2	0.0	0.0	68.2	68.2	22.9	68.2	1.5	10.4	0.1
2	20.8	32.3	0.0	0.0	0.0	0.0	68.2	68.2	22.8	68.2	0.8	2.3	0.1
3	0.0	0.0	0.0	0.0	0.0	0.0	68.2	68.2	0.5	68.2	0.0	0.0	0.1
4	0.0	0.0	0.0	0.0	0.0	0.0	0.0	0.0	0.0	0.0	0.0	0.0	0.1

Table A1-8. Fuel Oxidation Simulation Data for Case 8 (Exponential Decomposition of the Residual Water in 72.2 Years, Thermal Decay Constant Equal to 0.064, Zircaloy-4 Cladding)

Zone	Low-End Fuel and Cladding Initial Temperatures						High-End Fuel and Cladding Initial Temperatures						Cladding Failure Rate
	Fuel burnup (GW-day/MTU) and residual water amount (moles)												
	40 GW–day/MTU		50 GW–day/MTU		62 GW–day/MTU		40 GW–day/MTU		50 GW–day/MTU		62 GW–day/MTU		
	5.5 Moles	10 Moles	5.5 Moles	10 Moles	5.5 Moles	10 Moles	5.5 Moles	10 Moles	5.5 Moles	10 Moles	5.5 Moles	10 Moles	
	U_3O_8 Mass (g)	U_3O_8 Mass (g)	U_3O_8 Mass (g)	U_3O_8 Mass (g)	U_3O_8 Mass (g)	U_3O_8 Mass (g)	U_3O_8 Mass (g)	UO_{2+x} Mass (g)	U_3O_8 Mass (g)	U_3O_8 Mass (g)	U_3O_8 Mass (g)	U_3O_8 Mass (g)	
1	0.2	14.1	0.0	0.1	0.0	0.0	0.3	3.9	0.2	0.3	0.1	0.2	0.1
2	0.0	0.0	0.0	0.0	0.0	0.0	0.2	0.4	0.1	0.2	0.1	0.1	0.1
3	0.0	0.0	0.0	0.0	0.0	0.0	0.1	0.2	0.0	0.1	0.0	0.0	0.1
4	0.0	0.0	0.0	0.0	0.0	0.0	0.0	0.0	0.0	0.0	0.0	0.0	0.1

Table A1-9. Fuel Oxidation Simulation Data for Case 9 (Exponential Decomposition of the Residual Water in 4.8 Years, Thermal Decay Constant Equal to 0.064, ZIRLO Cladding)

Zone	Low-End Fuel and Cladding Initial Temperatures						High-End Fuel and Cladding Initial Temperatures						Cladding Failure Rate
	Fuel burnup (GW-day/MTU) and residual water amount (moles)												
	40 GW–day/MTU		50 GW–day/MTU		62 GW–day/MTU		40 GW–day/MTU		50 GW–day/MTU		62 GW–day/MTU		
	5.5 Moles	10 Moles	5.5 Moles	10 Moles	5.5 Moles	10 Moles	5.5 Moles	10 Moles	5.5 Moles	10 Moles	5.5 Moles	10 Moles	
	U_3O_8 Mass (g)	U_3O_8 Mass (g)	U_3O_8 Mass (g)	U_3O_8 Mass (g)	U_3O_8 Mass (g)	U_3O_8 Mass (g)	U_3O_8 Mass (g)	UO_{2+x} Mass (g)	U_3O_8 Mass (g)	U_3O_8 Mass (g)	U_3O_8 Mass (g)	U_3O_8 Mass (g)	
1	68.2	68.2	68.2	68.3	0.0	0.0	68.2	68.2	68.2	68.2	24.7	68.2	0.1
2	21.6	33.0	0.0	0.0	0.0	0.0	68.2	68.2	68.2	68.2	23.5	68.3	0.1
3	0.0	0.0	0.0	0.0	0.0	0.0	68.2	68.2	23.0	68.2	0.0	0.0	0.1
4	0.0	0.0	0.0	0.0	0.0	0.0	0.0	0.0	0.0	0.0	0.0	0.0	0.1

Table A1-10. Fuel Oxidation Simulation Data for Case 10 (Exponential Decomposition of the Residual Water in 72.2 Years, Thermal Decay Constant Equal to 0.064, ZIRLO Cladding)

Zone	Low-End Fuel and Cladding Initial Temperatures						High-End Fuel and Cladding Initial Temperatures						Cladding Failure Rate
	Fuel burnup (GW-day/MTU) and residual water amount (moles)												
	40 GW–day/MTU		50 GW–day/MTU		62 GW–day/MTU		40 GW–day/MTU		50 GW–day/MTU		62 GW–day/MTU		
	5.5 Moles	10 Moles	5.5 Moles	10 Moles	5.5 Moles	10 Moles	5.5 Moles	10 Moles	5.5 Moles	10 Moles	5.5 Moles	10 Moles	
	U_3O_8 Mass (g)	U_3O_8 Mass (g)	U_3O_8 Mass (g)	U_3O_8 Mass (g)	U_3O_8 Mass (g)	U_3O_8 Mass (g)	U_3O_8 Mass (g)	UO_{2+x} Mass (g)	U_3O_8 Mass (g)	U_3O_8 Mass (g)	U_3O_8 Mass (g)	U_3O_8 Mass (g)	
1	0.2	25.9	0.0	0.1	0.0	0.0	0.3	38.5	0.2	0.4	0.1	0.2	0.1
2	0.0	0.0	0.0	0.0	0.0	0.0	0.2	16.0	0.1	0.2	0.1	0.1	0.1
3	0.0	0.0	0.0	0.0	0.0	0.0	0.1	0.2	0.0	0.1	0.0	0.0	0.1
4	0.0	0.0	0.0	0.0	0.0	0.0	0.0	0.0	0.0	0.0	0.0	0.0	0.1

Table A1-11. Fuel Oxidation Simulation Data for Case 11 (Exponential Decomposition of the Residual Water in 4.8 Years, Thermal Decay Constant Equal to 0.064, M5 Cladding)

Zone	Low-End Fuel and Cladding Initial Temperatures						High-End Fuel and Cladding Initial Temperatures						Cladding Failure Rate
	Fuel burnup (GW-day/MTU) and residual water amount (moles)												
	40 GW–day/MTU		50 GW–day/MTU		62 GW–day/MTU		40 GW–day/MTU		50 GW–day/MTU		62 GW–day/MTU		
	5.5 Moles	10 Moles	5.5 Moles	10 Moles	5.5 Moles	10 Moles	5.5 Moles	10 Moles	5.5 Moles	10 Moles	5.5 Moles	10 Moles	
	U_3O_8 Mass (g)	U_3O_8 Mass (g)	U_3O_8 Mass (g)	U_3O_8 Mass (g)	U_3O_8 Mass (g)	U_3O_8 Mass (g)	U_3O_8 Mass (g)	UO_{2+x} Mass (g)	U_3O_8 Mass (g)	U_3O_8 Mass (g)	U_3O_8 Mass (g)	U_3O_8 Mass (g)	
1	68.2	68.2	68.2	68.2	0.0	0.0	68.2	68.3	68.2	68.3	68.2	68.3	0.1
2	21.6	33.0	0.0	0.0	0.0	0.0	68.2	68.2	68.2	68.2	68.2	68.3	0.1
3	0.0	0.0	0.0	0.0	0.0	0.0	68.2	68.2	23.1	68.2	0.0	0.0	0.1
4	0.0	0.0	0.0	0.0	0.0	0.0	0.0	0.0	0.0	0.0	0.0	0.0	0.1

Table A1-12. Fuel Oxidation Simulation Data for Case 12 (Exponential Decomposition of the Residual Water in 72.2 Years, Thermal Decay Constant Equal to 0.064, M5 Cladding)

Zone	Low-End Fuel and Cladding Initial Temperatures						High-End Fuel and Cladding Initial Temperatures						Cladding Failure Rate
	Fuel burnup (GW-day/MTU) and residual water amount (moles)												
	40 GW–day/MTU		50 GW–day/MTU		62 GW–day/MTU		40 GW–day/MTU		50 GW–day/MTU		62 GW–day/MTU		
	5.5 Moles	10 Moles	5.5 Moles	10 Moles	5.5 Moles	10 Moles	5.5 Moles	10 Moles	5.5 Moles	10 Moles	5.5 Moles	10 Moles	
	U_3O_8 Mass (g)	U_3O_8 Mass (g)	U_3O_8 Mass (g)	U_3O_8 Mass (g)	U_3O_8 Mass (g)	U_3O_8 Mass (g)	U_3O_8 Mass (g)	UO_{2+x} Mass (g)	U_3O_8 Mass (g)	U_3O_8 Mass (g)	U_3O_8 Mass (g)	U_3O_8 Mass (g)	
1	0.2	28.2	0.0	0.1	0.0	0.0	0.3	42.2	0.2	0.4	0.1	0.2	0.1
2	0.0	0.0	0.0	0.0	0.0	0.0	0.2	21.2	0.1	0.2	0.1	0.1	0.1
3	0.0	0.0	0.0	0.0	0.0	0.0	0.1	0.2	0.0	0.1	0.0	0.0	0.1
4	0.0	0.0	0.0	0.0	0.0	0.0	0.0	0.0	0.0	0.0	0.0	0.0	0.1